Post-collisional Pan-African granitoids and rare metal pegmatites in western Nigeria: age, petrogenesis, and the 'pegmatite conundrum'

K.M. Goodenough[1,*], P.A.J. Lusty[2], N. M. W. Roberts[3], R.M. Key[1], and A. Garba[4].

1: British Geological Survey, West Mains Road, Edinburgh EH9 3LA, UK

*: corresponding author: kmgo@bgs.ac.uk, +44 131 6500272

2: British Geological Survey, Environmental Science Centre, Keyworth, Nottingham, NG12 5GG, UK

3: NERC Isotope Geosciences Laboratory, Environmental Science Centre, Keyworth, Nottingham, NG12 5GG, UK

4: Nigerian Geological Survey Agency, 31 Shettima A Munguno Crescent, Utako, Abuja, Nigeria

Abstract

The Minna area of western Nigeria lies within a Pan-African orogenic belt that extends along the margin of the West African Craton, from Algeria southwards through Nigeria, Benin and Ghana, and into the Borborema Province of Brazil. This belt is characterised by voluminous post-collisional granitoid plutons that are well exposed around the city of Minna. In this paper we present new information about their age and petrogenesis.

The Pan-African plutons around Minna can be divided into two main groups: a group of largely peraluminous biotite-muscovite granites that show varying levels of deformation in late Pan-African shear zones; and a younger group of relatively undeformed, predominantly metaluminous hornblende granitoids. Pegmatites, including both barren and rare-metal types, occur at the margins of some of the plutons.

New U-Pb zircon dating presented here, in combination with published data, indicates an early phase of magmatism at c. 790-760 Ma in the Minna area. This magmatism could be related either to continental rifting, or to subduction around the margins of an existing continent. The peraluminous biotite-muscovite granites were intruded at

c. 650-600 Ma during regional shearing in the orogenic belt, and are likely to have formed largely by crustal melting. Subsequent emplacement of metaluminous granitoids at c. 590 Ma indicates the onset of post-orogenic extension in this area, with a contribution from mantle-derived magmas. The rare-metal pegmatites represent the youngest intrusions in this area and thus are likely to have formed in a separate magmatic episode, post-dating granite intrusion.

Keywords

Nigeria; Pan-African granite; post-collisional; rare-metal pegmatite; critical metals

1. Introduction

A network of Pan-African orogenic belts, formed during the Neoproterozoic to Cambrian amalgamation of Gondwana, extends across the African continent and into the Brasiliano orogen of South America (Black and Liégeois, 1993; Castaing et al., 1994; de Wit et al., 2008; Jacobs and Thomas, 2004; Stern, 1994). These belts are typically composed of Archaean and Proterozoic rocks that were reworked by Neoproterozoic to Cambrian orogenesis, together with a variable proportion of juvenile material. Many of the belts are characterised by extensive post-collisional granitoid plutons (Black and Liégeois, 1993; Küster and Harms, 1998). These plutons are typically potassic and their parental magmas are likely to be derived from mixed mantle and crustal sources (Black and Liégeois, 1993; Bonin, 2004; Küster and Harms, 1998; Liégeois et al., 1998). They thus represent major additions to the upper crust during amalgamation of Gondwana.

Alkaline igneous plutons, including those in post-collisional settings, are increasingly of interest as potential sources of ‘critical metals’ used in a range of advanced technologies. These critical metals include the Rare Earth Elements (REE), niobium and tantalum, which are commonly enriched in alkaline magmas. The increase in demand for these metals makes a reappraisal of the controls on magmatism and the potential for mineralisation worthwhile.

In West Africa, the Pan-African Dahomeyide orogenic belt separates the Archaean to Mesoproterozoic West African and Congo cratons, and is exposed in an area known as the Benin-Nigeria Shield (Ajibade and Wright, 1989). Northwards, this belt continues into the Hoggar Massif of Algeria; southwards, prior to Atlantic opening, it was connected to the Borborema Province of north-east Brazil (Arthaud et al., 2008; Caby, 1989; Castaing et al., 1994; Dada, 2008; de Wit et al., 2008; Neves, 2003).

In Nigeria, the Dahomeyide orogenic belt has been divided into eastern and western terranes separated by a major north-south lineament that has been recognised from remote sensing, but not studied in detail (Ajibade et al., 1987; Ananaba and Ajakaiye, 1987; Ferré et al., 1996; Fitches et al., 1985; Woakes et al., 1987) (Figure 1). The basement of the western terrane is dominated by Archaean migmatitic gneisses, with Proterozoic schist belts composed of low-metamorphic grade, highly deformed, metasedimentary and metavolcanic rocks (Ajibade et al., 1987; Arthaud et al., 2008; Bruguier et al., 1994; Dada, 2008; Fitches et al., 1985). The eastern terrane is characterised by high-grade (high-temperature amphibolite to granulite-facies), migmatitic metamorphic rocks that have Palaeoproterozoic protoliths but were migmatised during the Neoproterozoic (Ajibade et al., 1987; Ferré et al., 1996; Ferré et al., 2002). Proterozoic schist belts are not recognised in the eastern terrane. Both terranes are cut by a number of NNE–SSW-trending ductile shear zones that are tens to hundreds of kilometres in length, and can be correlated with similar shear zones in the Borborema Province in Brazil (Caby, 1989; Ferré et al., 2002).

Neoproterozoic magmatism at c. 780–770 Ma has been recorded in volcano-sedimentary sequences of the Borborema Province. This has been interpreted as related either to active subduction around continental margins, or to rifting (Arthaud et al., 2008; Fetter et al., 2003). Magmatism of this age has been recorded by relatively imprecise Rb-Sr dating in western Nigeria (Fitches et al., 1985).

The Nigerian basement is intruded by many Pan-African syn- to post-collisional plutons, which are more voluminous in the eastern terrane than the west, and which are known as the Older Granites. In eastern Nigeria, two suites of Older Granite plutonism have been recognised; an earlier (c. 640–600 Ma) suite of peraluminous biotite-muscovite granites, and a later (c. 600–580 Ma) suite of trans-alkaline hornblende-biotite granitoids (Ferré et al., 1998; Ferré et al., 2002). Emplacement of the later group was typically controlled by regional NE–SW shear zones (Ferré et al., 1995). The Older Granites of the western terrane were considered to be I-type granitoids by Fitches et al. (1985) but have not previously been subdivided into suites. Hornblende-biotite granites from the western terrane have been dated at c. 630-580 Ma, similar to those in eastern Nigeria (Key et al., 2012; Tubosun et al., 1984).

Within the eastern terrane, a suite of Mesozoic alkaline plutons emplaced in an intra-plate setting are known as the Younger Granites (Bowden, 1970). Mesozoic plutons have not been recognised in the western terrane.

Similar groups of Neoproterozoic granites have been recognised in the Borborema Province, where granitoid intrusions, including some S-type granites, were emplaced prior to or during the early stages of collision at c. 630–610 Ma. This was followed by emplacement of late-tectonic plutons, typically intruded into major shear zones, at 590–570 Ma (Arthaud et al., 2008; Bueno et al., 2009; Fetter et al., 2003; Neves et al., 2008). Contemporaneous granitoid plutons are also found in the Pan-African belts to the west and north of Nigeria. Westwards, in Ghana, Togo, and Benin, the overall period of granitoid magmatism lasted from c. 660–550 Ma (Kalsbeek et al., 2012) and alkaline plutons were emplaced at c. 590 Ma (Nude et al., 2009). To the north, in the Hoggar Massif of Algeria, alkaline post-collisional magmatism continued until c. 530 Ma (Caby, 2003)

The post-collisional granites in Nigeria are associated with rare metal (tin-tantalum) granitic pegmatites, some of which have been artisanally mined (Adetunji and Ocan, 2010; Garba, 2003; Kinnaird, 1984; Kuster, 1990; Matheis and Caen-Vachette, 1983; Melcher et al., 2013; Okunlola, 2005; Woakes et al., 1987). The rare metal pegmatites occur in a distinct belt that extends SW–NE from Ife to Jos, and appears to cut across the boundary between the eastern and western Nigerian terranes, although the individual pegmatite intrusions are oriented north-south (Kinnaird, 1984; Matheis and Caen-Vachette, 1983; Woakes et al., 1987). Individual pegmatites vary in length from 10 m to over 2 km, and can be up to 200 m wide (Adetunji and Ocan, 2010). Pegmatites of this type are typically associated with peraluminous or S-type granites (Cerny et al., 2012) and in western Nigeria the pegmatites are most commonly found close to the margins of peraluminous granite plutons. However, dating indicates that the pegmatites were emplaced at 560–450 Ma (Matheis and Caen-Vachette, 1983; Melcher et al., 2013), rather younger than the few previous dates for western Nigeria granites (Tubosun et al., 1984). The origin of these pegmatites is thus uncertain, although the peraluminous plutons with which they are associated have not previously been targeted for dating. Similar pegmatites occur in the Borborema Province, where they are extensively mined for tantalum (Beurlen et al., 2008). As well as the tantalum potential, gold deposits are known in the Nigerian schist belts, but their formation may pre-date the Pan-African orogeny (Dada, 2008).

Recent British Geological Survey (BGS) – Nigerian Geological Survey Agency (NGSA) geochemical mapping in the western Nigeria terrane (Key et al., 2012; Lapworth et al., 2012) has highlighted areas of enrichment in some critical metals, such as the Rare Earth Elements (REE), niobium and tantalum, around the Older Granite intrusions. This paper presents a more detailed study of these granitoids to investigate their age relationships, petrogenesis and potential for critical metal enrichment.

2. Geology of the study area

The area chosen for this study extends north-west from Abuja, the federal capital of Nigeria, and is centred on the city of Minna (Figure 2). This area lies within the western Nigeria terrane, and is a lush and well-vegetated part of Nigeria, made up of low rolling hills with rockier whalebacks forming on the Older Granites (Figure 3a). The basement comprises Archaean migmatitic gneisses with areas of Proterozoic schist and metavolcanic rocks (Ferré et al., 1996). The migmatitic gneisses in the study area are highly deformed, with the melanosome dominated by biotite and more than one phase of pegmatitic, quartzofeldspathic leucosome. The metavolcanic and metasedimentary rocks have been metamorphosed at greenschist to amphibolite facies.

The basement rocks are transected by a number of broadly north-south to NNE-SSW shear zones, the widest of which is defined by the outcrops of mylonites along the Zungeru River to the north-west of Minna (Figure 2). The rocks within this several-km wide Zungeru shear zone are intensely deformed, with a strong, steeply dipping, mylonitic foliation and a near-horizontal lineation (Fitches et al., 1985). They have a range of protoliths, including amphibolite and quartzofeldspathic rocks; the Older Granites are also intensely deformed in this shear zone (Figure 3b). A second major shear zone can be traced over a distance of around 100 km from the town of Kaduna SSW through Sarkin Pawa. It is marked by a zone at least several hundred metres wide in which the Older Granites and the country rocks are intensely foliated.

The Older Granites form between 30 and 40% of the outcrop area in the western Nigeria terrane (Fitches et al., 1985), and crop out extensively in the Minna area. They range from batholiths up to tens of km across to much smaller bodies (Figure 2). Previous work has indicated that syn-tectonic plutons are typically elongate parallel to the main regional NNE trend, whereas late-tectonic bodies tend to be rounded in shape (Ferré et al., 1998). There has been little or no previous detailed study of the plutons around Minna.

The Older Granites in the Minna area show a wide range of compositions, from diorite through monzonite and granodiorite to voluminous granite and rare syenite. They are typically coarse-grained, and many examples contain large (1 cm or more) white or pink tabular feldspars. Xenoliths of country rock are common at pluton margins. Later, cross-cutting sheets of aplitic and pegmatitic granite are also common. Three granite samples from the plutons north of Minna have previously been dated (by LA-ICPMS for U-Pb on zircons) at c. 606–616 Ma. All three samples were taken close to the major Zungeru and Sarkin Pawa shear zones (Key et al., 2012). A U-Pb age of 635 Ma has also been reported for a syn-tectonic granitoid from Sarkin Pawa (Dada, 2008).

Some of the plutons are elongate in a NNE-SSW trend, parallel to the major shear zones, and appear to have been emplaced during movement on those shear zones. These plutons show a gradation in deformation state. Some have a magmatic fabric defined by elongate tabular feldspars, but have not been-affected by solid state deformation. This magmatic fabric can grade into a moderate deformation fabric in which biotite plates and ribbons of quartz are aligned and xenoliths, where seen, are foliation-parallel. The most deformed granitoids have a pervasive fabric in which a gneissose banding has begun to develop, feldspars have been deformed and elongated, and all minerals define the tectonic foliation. Excellent examples of all these fabrics can be seen in the Tegina Pluton north-west of Minna, which lies within the Zungeru shear zone (Figure 2, 3b). This pluton consists of foliated biotite granite and granodiorite with some late pegmatite sheets.

Other plutons are not elongated parallel to the regional trend and their margins cross-cut the main fabric in their country rocks, although an intense deformation fabric is still developed where the granites are cut by localised shear zones. A particular example of this is the major Minna Batholith centred on the city of Minna. It comprises coarse-grained biotite-muscovite granite that is largely structureless or has a weak magmatic foliation, although numerous discrete, metre- to decametre-scale shear zones (typically with a NNE-SSW foliation) are present. Enclaves of biotite-rich country rock are common at the margins of the Minna Batholith.

Numerous smaller plutons of biotite-muscovite granite and granodiorite are found in the area around Sarkin Pawa north-east of Minna. These are commonly quite complex, with outcrops showing several magmatic phases from diorite through granodiorite to granite. In some areas these different phases have sharp but lobate contacts indicating magma mingling, whereas in others they have gradational contacts suggesting localised magma mixing. Late veins and sheets of pegmatite, aplite and leucogranite are abundant (Figure 3c). The granites and granodiorites are locally strongly foliated, particularly in the main Sarkin Pawa shear zone.

The Abuja Batholith forms a large mass that is not elongated parallel to regional shear zones. This batholith largely comprises pink, coarse-grained, alkali feldspar-rich hornblende-biotite granite with many enclaves and larger bodies of more mafic monzonitic to dioritic composition (Figure 3d). At some localities, the enclaves are rounded and have clear reaction rims with the granite but no evidence of chilling, indicating largely coeval magmatism. Biotite-muscovite leucogranites occur at the margins of the batholith; these have not been studied in detail, but may represent partially melted country rock as suggested for similar plutons in eastern Nigeria (Ferré et al., 1998).

Mineralised pegmatites are associated with the Older Granite plutons in Nigeria, and existing Rb-Sr dates suggest that the pegmatites in central Nigeria were emplaced at c. 555 Ma (Matheis and Caen-Vachette, 1983). These pegmatites form sheets, typically up to 1-2 m wide, cutting both basement rocks and the Pan-African granitoid plutons. In some areas, much larger pegmatitic bodies up to 200 m wide have been recognised (Adetunji and Ocan, 2003). The pegmatite suite can be divided into ‘barren’ and ‘rare metal’ suites (Garba, 2003). The rare metal pegmatites comprise quartz, K-feldspar, plagioclase, muscovite, biotite, and tourmaline with varying amounts of beryl, lepidolite, spodumene, garnet, apatite and accessory minerals including columbite – tantalite, tapiolite, wodginite, microlite, ilmenite and cassiterite (Melcher et al., 2013; Wright, 1970). Crystals can vary up to 5 cm in size. The accessory minerals are worked for tantalum by artisanal miners. The barren pegmatites comprise quartz, K-feldspar, plagioclase, muscovite and biotite, but lack the accessory minerals that concentrate rare metals. Both barren and rare metal pegmatites are found in the Minna area, typically close to the biotite-muscovite granite plutons.

3. Petrography of the granitoids

The Older Granites in the study area share a number of petrological features; they are typically coarse-grained, and primary magmatic crystal shapes are rare; textures range from granoblastic and equigranular, to strongly foliated with aligned mafic minerals and quartz ribbons. However, each of the named batholiths in the study area (Figure 2) is characterised by slightly different mineralogy and petrology.

The Minna Batholith is largely composed of coarse-grained leucogranites, generally with c. 10% mafic minerals. Large (up to 1 cm), subhedral plates of heavily sericitised microcline and plagioclase, zoned in some samples, are set in a matrix of recrystallized pools of quartz with smaller feldspar crystals. The main mafic minerals are biotite and muscovite, with primary epidote or zoisite and garnet in a few samples. Cross-cutting aplites and pegmatites have similar mineralogy but vary in grain size. Where these granitoids are sheared, a foliation is defined by aligned flakes of biotite and muscovite, and ribbons of recrystallized quartz (Figure 4a). Larger epidote crystals are undeformed, and wrapped by the foliation.

The Tegina Pluton shows significant variation in deformation state. It is formed of coarse-grained biotite granite, granodiorite and diorite, with 10–30% mafic minerals. Large subhedral feldspar (microcline and/or plagioclase) plates have very ragged, recrystallized rims, and quartz is also recrystallized to granoblastic textures, forming distinct elongate ribbons in more sheared samples. Biotite is the main mafic mineral, with hornblende and garnet also being present in the more mafic granodiorite (Figure 4b). Biotite flakes are aligned and define the foliation in sheared samples. One sample contains euhedral, zoned allanite crystals up to 2 mm across associated with clusters of biotite.

Plutons around Sarkin Pawa are largely made up of leucogranite with numerous shear zones. Large plates of microcline (2–10 mm across) are common in a matrix of recrystallized quartz with alkali feldspar and plagioclase. Mafic minerals are generally less than 15% of the rock; biotite is the main mafic mineral and muscovite is also present in most samples. Hornblende, garnet, titanite, and zircon all occur in some samples. Samples from shear zones have a foliation defined by elongate micas and pools of recrystallized quartz, typically wrapping around rounded plates of microcline. Late leucogranite and pegmatitic granite sheets are common in this area. A leucogranite sheet cross-cutting foliated granitoids close to Sarkin Pawa village contains hornblende and euhedral, zoned allanites up to 0.5 mm across (Figure 4c). Rare-metal pegmatites occur close to the pluton margins around Sarkin Pawa, cutting both the granites and the country rocks; some have granite-like mineralogy and contain large tourmaline crystals, whereas other examples are composed almost entirely of quartz and lithium mica. Tantalite is a notable accessory mineral in these pegmatites.

The Abuja Batholith is dominated by biotite-amphibole granitoids; hornblende is the predominant amphibole, but more sodic compositions are also present. Feldspars in these rocks, most typically microcline, can form large crystals (up to 2 cm) and these commonly have very irregular, recrystallized rims. More mafic monzonitic to monzodioritic compositions, with up to 40% mafic minerals, were found particularly at a locality in the north of the batholith. Some samples from this locality include remnant orthopyroxene, which shows two stages of hydration and alteration, firstly to cummingtonite and then to hornblende (Figure 4d). The orthopyroxene-bearing compositions correspond to the hypersthene-quartz monzodiorites (also described as charnockites) of eastern Nigeria (Ferré et al., 1998). Accessory minerals found throughout the Abuja Batholith include titanite, apatite, zircon and opaque oxides.

4. Analytical methods

4.1 Whole-rock geochemistry

The samples comprised 2–3 kg of carefully selected representative rock chips. Preparation and analysis of the samples was carried out by Acme Analytical Laboratories Ltd, Vancouver. 1 kg of material was crushed before a 250 g split was taken for analysis. Samples were analysed for 11 major oxides by ICP-ES and 34 trace elements by ICP-MS, following a lithium borate fusion and dilute acid digestion of a 0.2 g sample to give total abundances. Due to the interest in metallogenesis, the samples were also analysed for 14 metallic elements by ICP-MS following a hot aqua regia digestion of 0.5 g samples. Duplicate analyses were within ± 2% of each other for major elements and key trace elements. Data for blanks were below detection limits; data for international standard SO-18 were consistent with accepted values. Data are presented in Table 1; data for elements that were consistently below detection limit have not been included, and these include many of the metallic elements analysed following the aqua regia digestion.

4.2 U-Pb Geochronology

Zircon crystals from four samples were dated by Laser Ablation Inductively Coupled Plasma Mass Spectrometry (LA-ICP-MS) using a New Wave Research 193ss Nd-YAG laser ablation system coupled to a Nu Instruments Attom single collector ICP-MS. The full analytical method is described in Thomas et al. (2013). Zircons were analysed in an epoxy mount after heavy mineral separation, and were imaged with cathodoluminescence to characterise growth zones. Laser ablation parameters include a 25 μm spot size, 2.5 j/cm^2 fluence, 30 second ablation time, 15 second washout time, and 60 second background measurement prior to each ~20 analyses. A standard sample bracketing routing was used to normalise Pb/U and Pb/Pb ratios using the zircon reference material 91500. Secondary zircon reference materials (GJ-1 and Plesovice) were analysed during the session to check accuracy and precision, both of which are <3% 2σ. The full analytical results are provided in the online supplementary files. All final crystallisation ages are $^{206}Pb/^{238}U$ ages, and include two uncertainties written as ± x/y, whereby x is the 2σ uncertainty after propagation of measurement and session-based uncertainties, and y is the 2σ total uncertainty after propagation of systematic uncertainties. The latter should always be referred to for age comparison and compilation.

5. Geochemistry of the granitoids

Forty-five whole-rock samples from the Minna, Abuja, Tegina and Sarkin Pawa intrusions were analysed for major, trace and rare earth elements (Table 1). The majority of samples are granite *sensu stricto* with SiO_2 >70 wt% (Figure 5a) with rarer monzonite, granodiorite and syenite. Three samples from within the Abuja Batholith have SiO_2 <60 wt% and plot in the monzonite field on a total alkali-silica diagram. In general the Abuja Batholith samples appear to follow a more alkaline evolution trend than samples from the other intrusions, with higher total alkalis ($Na_2O + K_2O$) at lower SiO_2 contents. Samples from the Abuja Batholith also fall within the high-K field on a K_2O vs SiO_2 plot (Figure 5b); samples from the Minna Batholith largely fall in the medium-K field, and samples from other plutons spread across the boundary between high and medium-K fields. MgO is generally low (< 2wt% in almost all samples) but total FeO + Fe_2O_3 is more variable. Samples from the Abuja Batholith, and some from the Sarkin Pawa plutons, are typically metaluminous; samples from the Minna Batholith, the Tegina Pluton, and most of the Sarkin Pawa plutons, are typically peraluminous (Figure 6). Figure 6 shows that the samples from the Abuja Batholith overlap with the fields for the later trans-alkaline granitoid suite in eastern Nigeria (Ferré et al., 1998). However, the samples from the other western Nigeria plutons extend to significantly more peraluminous compositions. Geochemical data for the peraluminous plutons of eastern Nigeria are not available for comparison.

The different intrusive complexes are clearly distinguished on well-established granite discrimination diagrams (Figure 7). On the Y vs Nb plot (Pearce et al., 1984), all samples from the Minna Batholith and Tegina plutons, as well as most Sarkin Pawa samples, plot within the field of volcanic arc and syn-collisional granites. Samples from the Abuja Batholith and some Sarkin Pawa plutons extend into the Within-Plate Granite field. Similarly, on the Ga/Al vs Zr discrimation plot (Whalen et al., 1987), the Minna and Tegina samples fall largely within the I- , S- and M-type field, whereas most of the Abuja Batholith samples lie within the A-type field. Samples from Sarkin Pawa extend across both fields. The samples from the Abuja Batholith typically overlap with the trans-alkaline granites and quartz-monzonites of eastern Nigeria (Ferré et al., 1998). Post-collisional granitoids are generally known to extend across more than one field in these diagrams (Pearce, 1996), reflecting the involvement of several different sources in their formation, including mixing of mantle and crustal sources.

On the plot of SiO_2 vs Fe* (Frost et al., 2001), samples from the Abuja Batholith fall entirely within the A-type or ferroan granite field, and samples from the other plutons fall entirely within the post-collisional granite field, although there is considerable overlap (Figure 8). Samples from the Minna Batholith and Sarkin Pawa plutons extend across the boundary between the ferroan and magnesian fields, indicating contributions from more than one source component.

Post-collisional granitoids throughout the Pan-African orogenic belts are typically characterised by similar geochemical features, including relatively high contents of the large-ion lithophile elements (LILE), negative Nb-Ta, Sr and Ti anomalies, and relative enrichment in the light REE (LREE) (Goodenough et al., 2010; Küster and Harms, 1998). Spider diagrams for representative granite samples from the western Nigeria plutons show many of these features (Figure 9). All the granites have minor relative enrichment in the LILE such as Rb, Ba and K; relative depletions in Ta, Nb and Ti; and enrichment of the LREE over the heavy REE (HREE). The most fractionated granitoids are typically more strongly enriched in the LREE over HREE and have negative Sr and Eu anomalies; a notable example of this is sample NG/11/12, a late leucogranite sheet from the Sarkin Pawa area.

Granite, granodiorite and monzonite samples from the Abuja Batholith typically show the least fractionated patterns and have higher contents of Nb, Ta, Zr, Hf and the HREE relative to samples from the other areas. However, it is notable that the more silica-rich granitic rocks from the Abuja Batholith actually have lower contents of many incompatible elements (including Nb, Ta, Zr, Hf , and the MREE and HREE) than the more mafic monzonitic rocks (Figure 9b). This suggests that the granitic and monzonitic compositions cannot be related by simple fractional crystallisation, which would enhance incompatible element contents in the most evolved magmas, and that they are likely to represent mixing of two magmatic components. The results of a simple mixing calculation, using the spreadsheet of Ersoy and Helvaci (2009), are presented in Figure 10a. The most mafic (monzonitic) component of the Abuja Batholith is represented by sample NG/11/45, and local crustal material is represented by sample NG/11/16, a bulk sample of western Nigeria Archaean migmatitic gneiss. It is evident that mixing with local crustal material has the potential to explain many of the observed geochemical patterns in the Abuja Batholith. However, it is important to note that NG/11/16 is a single sample and does not fully represent the variation of compositions in the local crust.

In general, the geochemical patterns of the Abuja Batholith are similar to those of the trans-alkaline plutons from Eastern Nigeria (Ferré et al., 1998) and from other Pan-African suites such as the Maevarano suite of Madagascar (Goodenough et al., 2010) (Figure 10b). However, samples of peraluminous granite from the Minna Batholith are generally characterised by lower contents of most incompatible elements than samples from the Abuja Batholith. These geochemical patterns, particularly low contents of Hf, Zr, Ta and Nb, cannot be explained by simple melting of the local Archaean gneisses. Petrography shows that the Minna Batholith samples are characterised by large plates of feldspar in a felsic matrix; such textures are unlikely to represent magmatic compositions, and thus it is difficult to derive source compositions from the whole-rock geochemistry. However, the peraluminous nature of these granitoids indicates a likely derivation from sedimentary sources, potentially those represented by the Proterozoic schist belts.

Total REE contents (TREE) vary up to 915 ppm (in fractionated leucogranite sheets from Sarkin Pawa) and are dominated by the LREE, with the highest TREE contents found in allanite-bearing samples. It is notable that TREE contents show a weak negative correlation with SiO_2, with some of the most evolved granitic rocks showing the lowest total REE contents.

Late pegmatites are found across the Minna area and have been recognised in spatial association with the Minna, Tegina and Sarkin Pawa plutons, both cutting the granite plutons and intruded around their margins. Of these, true rare-metal pegmatites have only been found by this study in association with the Sarkin Pawa plutons. All these late pegmatites have variable trace element patterns but are typically strongly fractionated. They are enriched in Rb, K, U, Nb and Ta relative to the granitoids, but typically show notable depletions in Ba, the REE, Hf and Zr (Figure 9). All have negative Ti anomalies, but Eu and Sr are more variable. The pegmatites are also characterised by notably higher Ta/Nb and Hf/Zr ratios than the granites; this is characteristic of highly evolved magmas of this type (Linnen, 1998). The rare metal pegmatites from the Sarkin Pawa area also have elevated Be, Cs, Sn and W contents (Table 1) and in this respect they are generally typical of the LCT (Li-Cs-Ta) family of pegmatites (Cerny and Ercit, 2005; Cerny et al., 2012). Similar whole-rock geochemical patterns for rare metal pegmatites and their host granites are known from other areas of post-collisional magmatism, such as the Altai mountains of China (Zhu et al., 2006), but there are very few published whole-rock geochemical data for pegmatites from the Pan-African orogenic belts.

6. Geochronology of the granitoids

Four samples of the plutonic rocks were collected for U-Pb dating by LA-ICPMS (Table 2). Sample NG/11/12 was collected from an allanite-bearing leucogranite sheet cross-cutting foliated granitoids in the Sarkin Pawa area, and represents the youngest magmatism in that area. Sample NG/11/25 is a strongly foliated granodiorite from the outer part of the Minna Batholith, and NG/11/35 is a garnetiferous biotite-muscovite granite also from the Minna Batholith. Sample NG/11/49 is a biotite granite from the Abuja Batholith.

6.1 Zircon Description and Interpretation

NG/11/12

Zircon in this sample comprises largely prismatic grains with length/width ratios of 1 to 4, showing complex oscillatory zoning, typically with darker inner zones and brighter outer zones under cathodoluminescence (CL) (Figure 11a). Unconformities in the zoning are observed in some grains (less than a third of the total population). Altered zoning in the form of convolutions of the oscillatory zones is also seen in some grains. Metamorphic rims are not apparent, but some of the outer zones are thin with embayments into the inner zones. The population looks consistent and would be expected to give one, or at most two main ages.

NG/11/25

This sample contains prismatic zircon grains with length/width ratios of 1 to 2 and complex oscillatory zoning, typically with one or two unconformities per grain (Figure 11b). Some grains (less than a third of the population) have fuzzy or convoluted inner zones. The inner zones typically appear darker under cathodoluminescence, and the outer zones appear brighter. Embayments or metamorphic rims are not apparent. Two or more magmatic growth periods may be recorded by this zircon population.

NG/11/35

Zircon grains in this sample are prismatic with length/width ratios of 1 to 3 (Figure 11c). They show complex oscillatory zoning, typically with darker outer zones under

CL. Most grains exhibit unconformities between outer and inner zones. Many grains (c. two-thirds of the population) exhibit alteration of the inner zones, generally in the form of convolution of zoning and/or a granular texture. Many outer zones have embayment, but no thin metamorphic rims are apparent. The population is probably comprised of at least two growth phases; alteration of the inner zones may be younger than zircon crystallisation, or part of the youngest growth phase.

NG/11/49

This sample contains prismatic zircon grains with length/width ratios of 2 to 4 (Figure 11d). Complex oscillatory zoning is ubiquitous. Darker outer zones around brighter inner zones are most common, but brighter outer zones also exist. Unconformities across zoning are present in some grains (less than a quarter of the population). Some convolution of zoning occurs on the outer zone of some grains, but this is typically associated with inclusions within the zircons. No metamorphic rims are apparent. Crystallisation probably occurred during one main magmatic episode, but discordant inner zones suggest the possibility of inherited zircon cores.

6. 2 Results

NG/11/12

62 analyses were made from 54 grains, 8 of these were rejected due to high common Pb component (>600 cps Pb^{204}). The data cluster around 590 Ma (Figure 12a). One concordant grain at ~1008 Ma ($^{207}Pb/^{206}Pb$ age) indicates some inheritance; this analysis was from a core of a grain. The data spread towards slightly older ages along Concordia. These may represent a slightly older inherited component, or mixing with distinctly older zones (e.g. ~1000 Ma); the latter is not supported by the CL imagery. The data also spread towards discordant analyses with older $^{207}Pb/^{206}Pb$ ages, these probably result from small amounts of common lead and/or mixing with inherited components. For the age calculation, discordant (>10%) analyses were excluded, as were distinctly older concordant analyses. The youngest analysis pertains to an outer zone of a grain that has an embayment to the inner zone, this was also excluded from the age calculation. The remaining 41 analyses give a weighted mean $^{206}Pb/^{238}U$ age of 590 ± 3/13 Ma (MSWD = 1.8).

NG/11/25

50 analyses were made from 46 zircon grains, and these cluster around 780–760 Ma (Figure 12b). One concordant grain at 830 Ma ($^{206}Pb/^{238}U$ age), indicates inheritance

of a slightly older component. Three discordant (>10%) analyses are likely affected by common lead, and/or mixing with an inherited component. The rest of the population spreads along concordia slightly, and exhibits some minor reverse discordance. The CL imagery resolved discordant zoning that indicates the likelihood of crystallisation during more than one phase. The data are split into inner and outer zones, although this includes some subjectivity since some grains do not have obvious boundaries between zones. Excluding one analysis with a high degree of reverse discordance, 19 outer zone analyses give a weighted mean $^{206}Pb/^{238}U$ age of 764 ± 6/18 Ma (MSWD = 1.7). The remaining 26 inner zone analyses overlap in age with a weighted mean $^{206}Pb/^{238}U$ age of 774 ± 7/19 Ma (MSWD = 3.9) but spread to much older ages. The age given by the outer zones is interpreted as representing final crystallisation of the unit.

NG/11/35

46 analyses were made from 38 zircon grains, and 4 of these were rejected due to high common Pb (>600 cps PB^{204}). One inherited grain is distinctly older then the main populations at ~2100 Ma. The rest of the data spread from ~820 to 620 Ma (Figure 12c), and include a range of analyses that extend to older $^{207}Pb/^{206}Pb$ ages, probably related to minor common Pb content. After exclusion of discordant (>10%) data, the analyses fall into two broad populations. The data have been divided into inner and outer zones based on the CL imagery. Nine of the ten inner zones form a population which gives a weighted mean $^{206}Pb/^{238}U$ age of 793 ± 12/21 Ma (MSWD = 2.9). Twelve of the thirteen outer zones form a population which gives a weighted mean $^{206}Pb/^{238}U$ age of 653 ± 12/19 Ma (MSWD = 6.3). These two populations both have a high MSWD, which indicates that they do not represent single populations, probably because the analyses represent a small amount of mixing between different age zones. The youngest phase of crystallisation of this unit is interpreted to be ca. 653 Ma, and an earlier crystallisation is recorded at ca. 793 Ma.

NG/11/49

Forty analyses were made from 30 zircon grains, and of these only one corresponds to a distinctly older inherited grain, dated at ca. 1180 Ma ($^{207}Pb/^{206}Pb$). The rest of the analyses cluster around an age of ~590 Ma (Figure 1
2d). Several analyses spread to slightly older $^{207}Pb/^{206}Pb$ ages, probably related to a minor common lead content. Three analyses are slightly older than the main population in terms of $^{207}Pb/^{206}Pb$ age; one of these is slightly normally discordant

and dated at 639 Ma ($^{206}Pb/^{238}U$ age), and two are reversely discordant and dated at 620 Ma ($^{206}Pb/^{238}U$ age). These older analyses indicate the possibility of a slightly older inherited component, but do not particularly relate to separate internal zones that are apparent from the CL imagery. The remaining 30 analyses define a single population with a weighted mean $^{206}Pb/^{238}U$ age of 588 ± 3/13 Ma (MSWD = 1.07). This is interpreted as dating crystallisation of this unit.

7. Discussion

Field, petrological and geochemical data for Pan-African granitoids in the Minna area clearly indicate that the granitoid plutons can be divided into two broad groupings. The Minna Batholith, the Tegina Pluton and plutons around Sarkin Pawa comprise biotite-muscovite granites, locally containing garnet and epidote, which typically have peraluminous compositions. They show evidence of having been emplaced into an active tectonic regime characterised by major NNE-SSW shear zones. The second grouping comprises the metaluminous hornblende granitoids of the Abuja Batholith and late intrusive sheets in the Sarkin Pawa area. These intrusions are more alkaline, and contain a greater mafic magmatic component than the earlier biotite granites, varying from syenodiorites to leucogranites. In general they have higher contents of Nb, Zr and Hf than the biotite granites, but this study has found no evidence for significant critical metal enrichments. A third group of intrusions, the late pegmatites, is found throughout much of the area and discussed separately from the major plutons.

The age data from this study, together with published ages of Key et al. (2012), indicate that the Older Granite magmatism in the Minna area spanned a considerable amount of time. The Minna Batholith clearly contains evidence for an early phase of magmatism at c. 790–760 Ma. Because one sample (NG/11/25) has a single population of zircons of this age, this is highly unlikely to represent an inheritance age, and is considered to date crystallisation of the unit. The sample was taken from an outcrop apparently within the Minna Batholith, but may represent a large screen of older crust that has been incorporated within the batholith, but not assimilated. Ages of c. 790–740 Ma have previously been obtained by relatively imprecise Rb-Sr dating of Nigerian Older Granites from the area north of Minna (Fitches et al., 1985), and magmatic ages of 800–770 Ma are found in the Borborema Province (Arthaud et al., 2008). The tectonic setting of the Brazilian magmatism is debated, and may be related to continental rifting, or to subduction at an active continental margin (Arthaud et al., 2008; de Araujo et al., 2012; Fetter et al., 2003). It is evident that Nigeria was affected by a contemporaneous magmatic event. However, only the single dated sample can be clearly attributed to this event in Nigeria. Identification and study of individual intrusions formed at this time would be needed in order to identify the tectonic setting.

The sites of earlier Neoproterozoic magmatism were subsequently exploited by later peraluminous magmas at c. 650 Ma, as demonstrated by the two age populations in sample NG/11/35. These earlier, biotite-muscovite peraluminous granites are likely to have had a significant source component of sedimentary material. However, a lack of published isotopic data means that the source of this sedimentary material remains in doubt; one potential source lies in the schist belts of the western Nigeria terrane. The magmas are thought to have formed by crustal melting associated with high-temperature metamorphism and crustal thickening following the peak of the main Pan-African collision (Ferré et al., 2002).

Biotite granites continued to be emplaced in the region between c. 635 and 600 Ma (Dada, 2008; Key et al., 2012), and in many areas these were affected by intense ductile shearing, acquiring strong syn- to post-magmatic foliations.

Subsequently, metaluminous hornblende granitoids were emplaced at c. 590 Ma, forming the Abuja Batholith as well as later leucogranite sheets in the Sarkin Pawa area (samples NG/11/12 and NG/11/49). Relatively mafic monzonitic to monzodioritic lithologies are present as enclaves and larger masses within the Abuja Batholith. In contrast with the earlier peraluminous granites, the metaluminous granitoids, monzonites and monzodiorites have alkaline affinities, and show many geochemical features akin to A-type granitoids. However, the presence of negative Nb-Ta anomalies is not typical of A-type granitoids, but can be attributed either to melting of a lithospheric mantle source that has been enriched by earlier subduction, or to contamination by continental crust.

Recent geochemical and isotopic studies of coeval metaluminous hornblende-biotite granitoids in eastern Nigeria show that initial ε_{Nd} ranges from -5 to -16, and initial $^{87}Sr/^{86}Sr$ ranges from 0.70617 to 0.71015 (Dada et al., 1995; Ferré et al., 1998). These data have been interpreted to indicate that the source of the granitoid magmas was largely in the continental crust, with limited contribution from the mantle (Dada et al., 1995). The more mafic components of the suite in eastern Nigeria are highly potassic quartz monzonites such as those in the Bauchi pluton (although the best available dates place these at c. 640 Ma (Dada and Respaut, 1989; Oyawoye, 1961)). Isotopic data for these monzonites show a trend towards more mantle-like compositions with initial ε_{Nd} from -4 to - 8 (Dada et al., 1995). Strongly alkaline c. 590 Ma intrusions sourced from mantle-derived magmas have also been recognised in the Dahomeyide belt in Ghana (Nude et al., 2009). Geochemical evidence in both eastern (Ferré et al., 1998) and western Nigeria (this study) indicates that the metaluminous granitoids were not formed by direct fractional crystallisation of the more mafic monzonitic and monzodioritic magmatic component. Instead, the composition of the granitoids can be largely explained by mixing between melts of the local Archaean meta-igneous crust, and a more mafic mantle-derived magma. Overall, the geochemical data for the metaluminous plutons of western Nigeria fit with the hypothesis proposed for similar plutons in eastern Nigeria, namely a fractionated mantle-derived magma that has mixed with magmas derived by melting of igneous material in the continental crust (Dada et al., 1995; Ferré et al., 1998).

The final magmatic event in the area was the intrusion of barren and rare-metal pegmatites, which have been dated at 560–450 Ma (Matheis and Caen-Vachette, 1983; Melcher et al., 2013). Late pegmatites are spatially associated with most of the Older Granite plutons, but the dating indicates that they post-date the Older Granites, and are not directly genetically related to them, as originally suggested by Matheis (1987). This is difficult to reconcile with the geochemical evidence presented here, which shows that the pegmatites formed from very highly evolved magmas. These pegmatites have affinities with the LCT pegmatite family, which is typically considered to comprise the most highly fractionated parts of S-type or peraluminous granitic suites formed during crustal thickening (Cerny et al., 2012). However, in western Nigeria the dating presented here indicates that the Older Granites evolved with time away from a sedimentary source towards an increased contribution from a mantle or lower crustal source. The origin of the pegmatites thus remains uncertain.

The Borborema Province in Brazil also contains rare-metal pegmatites emplaced at 515–509 Ma (Baumgartner et al., 2006); as with the Nigerian pegmatites, these have been artisanally mined for Nb and Ta. The Borborema Province pegmatites are also associated with granites, and as in Nigeria, the pegmatites appear to be distinctly younger than the granites. This ‘pegmatite conundrum’ has been recognised in post-collisional settings elsewhere in the world (e.g. the Altai Mountains (Zhu et al., 2006)). Rare-metal pegmatites are typically considered to crystallise from highly fractionated magmas, representing the latest intrusion stage in a granitic province (Cerny et al., 2012). However, in many areas, they appear to post-date the associated granitoid plutons by a significant period of time, and potentially represent a separate intrusive event. Pegmatites such as those in western Nigeria are an important part of the global tantalum resource, yet their genesis remains poorly understood, and further work is needed to understand the source of these unusual magmas.

8. Conclusions

Pan-African-Brasiliano orogenic belts extending around the West African Craton contain abundant post-collisional granitoids, which are recognised throughout West Africa and Brazil. The Minna area of western Nigeria provides good exposures of all elements of this magmatic province.

The earliest magmatism, at 790–760 Ma, is recorded by zircon cores and zones of intensely deformed granodiorite within the Minna Batholith. Magmatism of this age is known in the Borborema Province of Brazil, and has also been recognised by Rb-Sr dating in Nigeria. It may be related to Neoproterozoic subduction around the margins of the West African Craton, but more work is needed to fully characterise this magmatic episode.

Large volumes of peraluminous biotite granite were produced during crustal thickening at 600–650 Ma in western Nigeria. Emplacement of these plutons was focused along large-scale crustal shear zones and many of the plutons are intensely foliated. These granites typically have peraluminous characteristics and were largely derived by melting of local crust.

Later, post-tectonic metaluminous magmas (hornblende diorites, granodiorites and granites) were emplaced in an extensional post-collisional setting at c. 590 Ma. The association of mafic (dioritic) and felsic magmas, emplaced contemporaneously, and the more alkaline, LILE-enriched nature of those magmas, indicates both mantle-derived and crustally-derived magmatic components. Thus, initial post-collisional melting in this orogenic belt was focused in the thickened upper to middle crust, with the mantle-derived component increasing over time.

The last magmatic event in western Nigeria was the emplacement of LCT-type pegmatites, some of which are enriched in rare metals such as tantalum. On the basis of current evidence, these pegmatites were emplaced at c. 560–450 Ma, and significantly post-date the peraluminous granitoid plutons. These pegmatites thus cannot be highly evolved melts derived from a fertile, S-type, parental granite as is normally considered for LCT pegmatites. The origin of such rare-metal pegmatites thus presents an unsolved conundrum.

Acknowledgments

The Nigerian Geological Survey Agency is thanked for logistical support in the field in Nigeria. Martin Gillespie is thanked for his very constructive and helpful comments on an earlier draft. Mike Fowler and Eric Ferré are thanked for their thorough reviews, which have greatly improved the paper. The authors publish with the permission of the Executive Director of the British Geological Survey.

Figures

Figure 1: Simplified map of the geology of Nigeria, after Ferré et al. (1996) and Key et al. (2012). Box indicates the area shown in Figure 2.

Figure 2: Simplified map of the geology of the Minna area, after Key et al. (2012).

Figure 3: a) Granite whaleback hill in the Tegina Pluton, illustrating the typical scenery of the field area; b) Foliated granitoid demonstrating strong solid-state deformation, Tegina Pluton; c) Coarse-grained porphyritic granitoid cut by late granite pegmatite, Sarkin Pawa area; d) Outcrop showing mingling, mixing and localised shearing of dioritic and granitic magmas in the Abuja Batholith.

Figure 4: Photomicrographs of thin sections from Nigerian Older Granites, viewed in plane polarised light. a) Sheared granitoid from the Minna Batholith, with a foliation defined by aligned biotites (Bt) and recrystallised quartz (Qz) ribbons, and highly altered feldspar (Fsp); b) Granodiorite from the Tegina Pluton, containing biotite (Bt), hornblende (Hbl) and garnet (Grt); c) Late stage hornblende (Hbl)-biotite (Bt) granite sheet from the Sarkin Pawa area with large, high-relief, yellowish allanite (Aln) crystals (Aln); d) Monzonite from the Abuja Batholith containing altered orthopyroxene (Opx) typically rimmed by hornblende (Hbl).

Figure 5: a) Plot of total alkalis versus silica for all analysed samples from Nigerian Older Granites, divided by pluton. Fields from Gillespie and Styles (1999). Dashed line represents boundary between alkalic rocks above and subalkalic rocks below (Miyashiro, 1974); b): Plot of K_2O vs SiO_2 for all samples, with fields from Le Maitre (2002).

Figure 6: Shand Index plot for all analysed samples. A/NK = molar (Al_2O_3/(Na_2O + K_2O)); A/CNK = molar (Al_2O_3/(CaO + Na_2O + K_2O)). Fields for trans-alkaline plutons from Eastern Nigeria (Ferré et al., 1998) given for comparison.

Figure 7: Granite discrimination diagrams for all analysed samples. a) Nb vs Y plot after Pearce et al. (1984); b) Zr vs Ga/Al plot after Whalen et al. (1987). Fields for trans-alkaline plutons from Eastern Nigeria (Ferré et al., 1998) given for comparison.

Figure 8: Plot of SiO_2 vs $FeO^{tot}/(FeO^{tot}+MgO)$ for all analysed samples, with fields for A-type and post-collisional granitoids from Frost et al. (2001)

Figure 9: Primitive mantle-normalised trace element plots for selected samples from the different plutons within the study area. Normalising factors from McDonough and Sun (1995).

Figure 10a): Primitive mantle-normalised trace element plots for samples from the Abuja Batholith, with grey lines showing the calculated compositions achieved by mixing Abuja Batholith monzonite (NG/11/48) with local Archaean crust; b) Primitive mantle-normalised trace element plots for representative samples from the Minna Batholith and Abuja Batholith (this study), the Rahama Granite of Eastern Nigeria (Ferré et al., 1998), and the comparable Maevarano suite of Madagascar (Goodenough et al., 2010). Normalising factors from McDonough and Sun (1995).

Figure 11: Cathodoluminescence images for representative zircon crystals from the four geochronology samples

Figure 12: Zircon concordia plots for the four dated samples. a) NG/11/12; b) NG/11/25; c) NG/11/35; d) NG/11/49. Analyses in black are those used for age calculations; those in grey were rejected due to discordance or mixed age.

Tables

Table 1: Whole-rock geochemical data for all analysed samples

Table 2 (online supplementary data): U-Pb data for the four dated samples. Discordance = (1-((206Pb/238U)/(207Pb/206Pb)))*100. Concentrations in ppm are based on normalisation to 91500, based on 14.8ppm Pb, 30ppm Th and 81.2ppm U. ^{204}Pb, ^{206}Pb, ^{207}Pb, ^{208}Pb, ^{232}Th and ^{235}U in counts per second. ^{204}Pb is after subtraction of ^{204}Hg based on measurement of ^{202}Hg. Osci = oscillatory zoning. Analyses in black are those used for age calculations.

References

Adetunji, A., Ocan, O.O., 2010. Characterization and Mineralization Potentials of Granitic Pegmatites of Komu area, Southwestern Nigeria. Resource Geology 60, 87-97.

Ajibade, A.C., Woakes, M., Rahaman, M.A., 1987. Proterozoic crustal development in the Pan-African regime of Nigeria, in: Kroner, A. (Ed.), Proterozoic Lithospheric Evolution AGU, Washington DC.

Ajibade, A.C., Wright, J.B., 1989. The Togo-Benin-Nigeria Shield: evidence of crustal aggregation in the Pan-African belt. Tectonophysics 165, 125-129.

Ananaba, S.E., Ajakaiye, D.E., 1987. Evidence of tectonic control of mineralization in Nigeria from lineament density analysis. A Landsat study. International Journal of Remote Sensing 8, 1445-1452.

Arthaud, M.H., Caby, R., Fuck, R.A., Dantas, E.L., Parente, C.V., 2008. Geology of the northern Borborema Province, NE Brazil, and its correlation with Nigeria, NW Africa, in: Pankhurst, R.J., Trouw, R.A.J., Brito Neves, B.B., De Wit, M.J. (Eds.), West Gondwana: Pre-Cenozoic Correlations across the South Atlantic Region. Geological Society, London, Special Publication 294, pp. 49-67.

Baumgartner, R., Romer, R.L., Moritz, R., Sallet, R., Chiaradia, M., 2006. Columbite-tantalite bearing granitic pegmatites from the Serido Belt, Northeastern Brazil: Genetic constraints from U-Pb dating and Pb isotopes. The Canadian Mineralogist 44, 69-86.

Beurlen, H., da Silva, M.R.R., Thomas, R., Soares, D.R., Olivier, P., 2008. Nb–Ta–(Ti–Sn) oxide mineral chemistry as tracer of rare-element granitic pegmatite fractionation in the Borborema Province, Northeastern Brazil. Mineralium Deposita 43, 207-228.

Black, R., Liégeois, J.P., 1993. Cratons, mobile belts, alkaline rocks and continental lithospheric mantle; the Pan-African testimony. Journal of the Geological Society of London 150, 89-98.

Bonin, B., 2004. Do coeval mafic and felsic magmas in post-collisional to within-plate regimes necessarily imply two contrasting, mantle and crustal, sources? A review. Lithos 78, 1-24.

Bowden, P., 1970. Origin of the younger granites of northern Nigeria. Contributions to Mineralogy and Petrology 25, 153-162.

Bruguier, O., Dada, S.S., Lancelot, J.R., 1994. Early Archaean component (> 3.5 Ga) within a 3.05 Ga orthogneiss from northern Nigeria: U-Pb zircon evidence. Earth and Planetary Science Letters 125, 89-103.

Bueno, J.F., Oliveira, E.P., McNaughton, N.J., Laux, J.H., 2009. U-Pb dating of granites in the Neoproterozoic Sergipano Belt, NE Brazil: Implications for the timing and duration of continental collision and extrusion tectonics in the Borborema Province. Gondwana Research 15, 86-97.

Caby, R., 1989. Precambrian terranes of Benin-Nigeria and northeast Brazil and the Late Proterozoic south Atlantic fit, in: Dallmeyer, R.D. (Ed.), Terranes in the Circum-Atlantic Palaeozoic Orogens. Geological Society of America Special Paper 230, pp. 145-158.

Caby, R., 2003. Terrane assembly and geodynamic evolution of central-western Hoggar: a synthesis. Journal of African Earth Sciences 37, 133-159.

Castaing, C., Feybesse, J.L., Thieblemont, D., Triboulet, C., Chevremont, P., 1994. Palaeogeographical reconstructions of the Pan-African/ Brasiliano orogen: closure of an oceanic domain or intracontinental convergence between major blocks? Precambrian Research 69, 327-344.

Cerny, P., Ercit, T.S., 2005. The Classification of Granitic Pegmatites Revisited. The Canadian Mineralogist 43, 2005-2026.

Cerny, P., London, D., Novak, M., 2012. Granitic Pegmatites as Reflections of Their Sources. Elements 8, 289-294.

Dada, S.S., 2008. Proterozoic evolution of the Nigeria-Boborema province, in: Pankhurst, R.J., Trouw, R.A.J., Brito Neves, B.B., de Wit, M.J. (Eds.), West Gondwana: Pre-Cenozoic Correlations across the South Atlantic Region. Geological Society of London Special Publication 294 pp. 121-136.

Dada, S.S., Briqueu, L., Harms, U., Lancelot, J.R., Matheis, G., 1995. Charnockitic and monzonitic Pan-African series from north-central Nigeria: Trace-element and Nd, Sr, Pb isotope constraints on their petrogenesis. Chemical Geology 124, 233-252.

Dada, S.S., Respaut, J.P., 1989. La monzonite à fayalite de Bauchi (bauchite), nouveau témoin d'un magmatisme syntectonique pan-africain au nord du Nigeria. Comptes Rendus Academie Science de Paris 309, 887-892.

de Araujo, C.E.G., Cordani, U.G., Basei, M.A.S., Castro, N.A., Sato, K., Sproesser, W.M., 2012. U–Pb detrital zircon provenance of metasedimentary rocks from the Ceará Central and Médio Coreaú Domains, Borborema Province, NE-Brazil: Tectonic implications for a long-lived Neoproterozoic active continental margin. Precambrian Research 206-207, 36-51.
de Wit, M.J., Stankiewicz, J., Reeves, C., 2008. Restoring Pan-African-Brasiliano connections: more Gondwana control, less Trans-Atlantic corruption in: Pankhurst, R.J., Trouw, R.A.J., Brito Neves, B.B., De Wit, M.J. (Eds.), Pre-Cenozoic Correlations Across the South Atlantic Region. The Geological Society, London, pp. 399-412.
Ersoy, Y., Helvaci, C., 2009. FC–AFC–FCA and mixing modeler: A Microsoft Excel spreadsheet program for modeling geochemical differentiation of magma by crystal fractionation, crustal assimilation and mixing. Computers and Geosciences 36, 383-390.
Ferré, E.C., Caby, R., Peucat, J.J., Capdevila, R., Monie, P., 1998. Pan-African, post-collisional, ferro-potassic granite and quartz-monzonite plutons of Eastern Nigeria. Lithos 45, 225-279.
Ferré, E.C., Deleris, J., Bouchez, J.-L., Lar, A.U., Peucat, J.-J., 1996. The Pan-African reactivation of Eburnean and Archaean provinces in Nigeria: structural and isotopic data. Journal of the Geological Society of London 153, 719-728.
Ferré, E.C., Gleizes, G., Bouchez, J.-L., 1995. Internal fabric and strike-slip emplacement of the Pan-African granite of Solli Hills, northern Nigeria. Tectonics 14, 1205-1219.
Ferré, E.C., Gleizes, G., Caby, R., 2002. Obliquely convergent tectonics and granite emplacement in the Trans-Saharan belt of Eastern Nigeria: a synthesis. Precambrian Research 114, 199-219.
Fetter, A.H., dos Santos, T.J.S., Van Schmus, W.R., Hackspacher, P.C., Brito Neves, B.B., Arthaud, M.H., Neto, J.A.N., Wernick, E., 2003. Evidence for Neoproterozoic Continental Arc Magmatism in the Santa Quiteria Batholith of Ceara State, NW Borborema Province, NE Brazil: Implications for the Assembly of West Gondwana. Gondwana Research 6, 265-273.
Fitches, W.R., Ajibade, A.C., Egbuniwe, I.G., Holt, R.W., Wright, J.B., 1985. Late Proterozoic schist belts and plutonism in NW Nigeria. Journal of the Geological Society of London 142, 319-337.
Frost, B.R., Barnes, C.G., Collins, W.J., Arculus, R.J., Ellis, D.J., Frost, C.D., 2001. A Geochemical Classification for Granitic Rocks. Journal of Petrology 42, 2033-2048.
Garba, I., 2003. Geochemical discrimination of newly discovered rare-metal bearing and barren pegmatites in the Pan-African (600 ± 150 Ma) basement of northern Nigeria. Applied Earth Science (Trans. Inst. Min. Metall. B) 112, 287-292.
Gillespie, M.R., Styles, M.T., 1999. Rock Classification Scheme Volume 1, Classification of Igneous Rocks, British Geological Survey Research Report (2nd ed.). British Geological Survey, Keyworth, Nottingham.
Goodenough, K.M., Thomas, R.J., De Waele, B., Key, R.M., Schofield, D.I., Bauer, W., Tucker, R.D., Rafahatelo, J.-M., Rabarimanana, M., Ralison, A.V., Randriamananjara, T., 2010. Post-collisional magmatism in the central East African Orogen: The Maevarano Suite of north Madagascar. Lithos 116, 18-34.
Jacobs, J., Thomas, R.J., 2004. Himalayan-type indenter-escape tectonics model for the southern part of the late Neoproterozoic-early Palaeozoic East African-Antarctic orogen. Geology 32, 721-724.

Kalsbeek, F., Affaton, P., Ekwueme, B., Frei, R., Thrane, K., 2012. Geochronology of granitoid and metasedimentary rocks from Togo and Benin, West Africa: Comparisons with NE Brazil. Precambrian Research 196-197, 218-233.

Key, R.M., Johnson, C.C., Horstwood, M.S.A., Lapworth, D.J., Knights, K.V., Kemp, S.J., Watts, M.J., Gillespie, M., Adekanmi, M.A., Arisekola, T.M., 2012. Investigating high zircon concentrations in the fine fraction of stream sediments draining the Pan-African Dahomeyan Terrane in Nigeria. Applied Geochemistry 27, 1525-1539.

Kinnaird, J.A., 1984. Contrasting styles of Sn-Nb-Ta-Zn mineralization in Nigeria. Journal of African Earth Sciences 2, 81-90.

Kuster, D., 1990. Rare-metal pegmatites of Wamba, central Nigeria - their formation in relationship to late Pan-African granites. Mineralium Deposita 25, 25-33.

Küster, D., Harms, U., 1998. Post-collisional potassic granitoids from the southern and northwestern parts of the Late Neoproterozoic East African Orogen: a review. Lithos 45, 177-195.

Lapworth, D.J., Knights, K.V., Key, R.M., Johnson, C.C., Ayoade, E., Adekanmi, M.A., Arisekola, T.M., Okunlola, O.A., Backman, B., Eklund, M., Everett, P.A., Lister, R.T., Ridgway, J., Watts, M.J., Kemp, S.J., Pitfield, P.E.J., 2012. Geochemical mapping using stream sediments in west-central Nigeria: Implications for environmental studies and mineral exploration in West Africa. Applied Geochemistry 27, 1035-1052.

Le Maitre, R.W., 2002. Igneous Rocks: A classification and glossary of terms. Recommendations of the IUGS Subcommission on the Systematics of Igneous Rocks. Cambridge University Press.

Liégeois, J.P., Navez, J., Hertogen, J., Black, R., 1998. Contrasting origin of post-collisional high-K calc-alkaline and shoshonitic versus alkaline and peralkaline granitoids. The use of sliding normalization. Lithos 45, 1-28.

Linnen, R.L., 1998. The Solubility of Nb-Ta-Zr-Hf-W in Granitic Melts with Li and Li + F: Constraints for Mineralization in Rare Metal Granites and Pegmatites. Economic Geology 93, 1013-1025.

Matheis, G., 1987. Nigerian rare-metal pegmatites and their lithological framework. Geological Journal 22, 271-291.

Matheis, G., Caen-Vachette, M., 1983. Rb-Sr isotopic study of rare-metal bearing and barren pegmatites in the Pan-African reactivation zone of Nigeria Journal of African Earth Sciences 1, 35-40.

McDonough, W.F., Sun, S.-s., 1995. The Composition of the Earth. Chemical Geology 120, 223-253.

Melcher, F., Graupner, T., Gabler, H.-E., Sitnikova, M., Henjes-Kunst, F., Oberthur, T., Gerdes, A., Dewaele, S., 2013. Tantalum- (niobium-tin) mineralisation in African pegmatites and rare metal granites: Constraints from Ta-Nb oxide mineralogy, geochemistry and U-Pb geochronology. Ore Geology Reviews. http://dx.doi.org/10.1016/j.oregeorev.2013.09.003

Miyashiro, A., 1974. Volcanic rock series in island arcs and active continental margins American Journal of Science 274, 321-355.

Neves, S.P., 2003. Proterozoic history of the Borborema province (NE Brazil): Correlations with neighboring cratons and Pan-African belts and implications for the evolution of western Gondwana. Tectonics 22. 10.1029/2001TC001352

Neves, S.P., Bruguier, O., Bosch, D., da Saliva, J.M.R., Mariano, G., 2008. U–Pb ages of plutonic and metaplutonic rocks in southern Borborema Province (NE Brazil):

Timing of Brasiliano deformation and magmatism. Journal of South American Earth Sciences 25, 285-297.
Nude, P.M., Shervais, J.W., Attoh, K., Vetter, S.K., Barton, C., 2009. Petrology and geochemistry of nepheline syenite and related carbonate-rich rocks in the Pan-African Dahomeyide orogen, southeastern Ghana, West Africa. Journal of African Earth Sciences 55, 147-157.
Okunlola, O.A., 2005. Metallogeny of Tantalum-Niobium Mineralization of Precambrian pegmatites of Nigeria. Mineral Wealth 137, 38-50.
Oyawoye, M.O., 1961. On an Occurrence of Fayalite Quartz-Monzonite in the Basement Complex around Bauchi, Northern Nigeria. Geological Magazine 98, 473-482.
Pearce, J.A., 1996. Sources and settings of granitic rocks. Episodes 19, 120-125.
Pearce, J.A., Harris, N.B.W., Tindle, A.G., 1984. Trace element discrimination diagrams for the tectonic interpretation of granitic rocks. Journal of Petrology 25, 956-983.
Stern, R.J., 1994. Arc Assembly and continental collision in the Neoproterozoic East African orogeny - implications for the consolidation of Gondwana. Annual Reviews of Earth and Planetary Sciences 22, 319-351.
Thomas, R.J., Roberts, N.M.W., Jacobs, J., Bushid, A.M., Horstwood, M.S.A., Mruma, A., 2013. Structural and geochronological constraints on the evolution of the eastern margin of the Tanzania Craton in the Mpwapwa area, central Tanzania. Precambrian Research 224, 671-689.
Tubosun, I.A., Lancelot, J.R., Rahaman, M.A., Ocan, O.O., 1984. U-Pb Pan-African ages of two charnockite-granite associations from Southwestern Nigeria. Contributions to Mineralogy and Petrology 88, 188-195.
Whalen, J.B., Currie, K.L., Chappell, B.W., 1987. A-type granites: geochemical characteristics, discrimination and petrogenesis. Contributions to Mineralogy and Petrology 95, 407-419.
Woakes, M., Rahaman, M.A., Ajibade, A.C., 1987. Some metallogenetic features of the Nigerian Basement. Journal of African Earth Sciences 6, 655-664.
Wright, J.B., 1970. Controls of Mineralization in the Older and Younger Tin Fields of Nigeria. Economic Geology 65, 945-951.
Zhu, Y.-F., Zeng, Y., Gu, L., 2006. Geochemistry of the rare metal-bearing pegmatite No. 3 vein and related granites in the Keketuohai region, Altay Mountains, northwest China. Journal of Asian Earth Sciences 27, 61-77.

Figure 1
Click here to download high resolution image

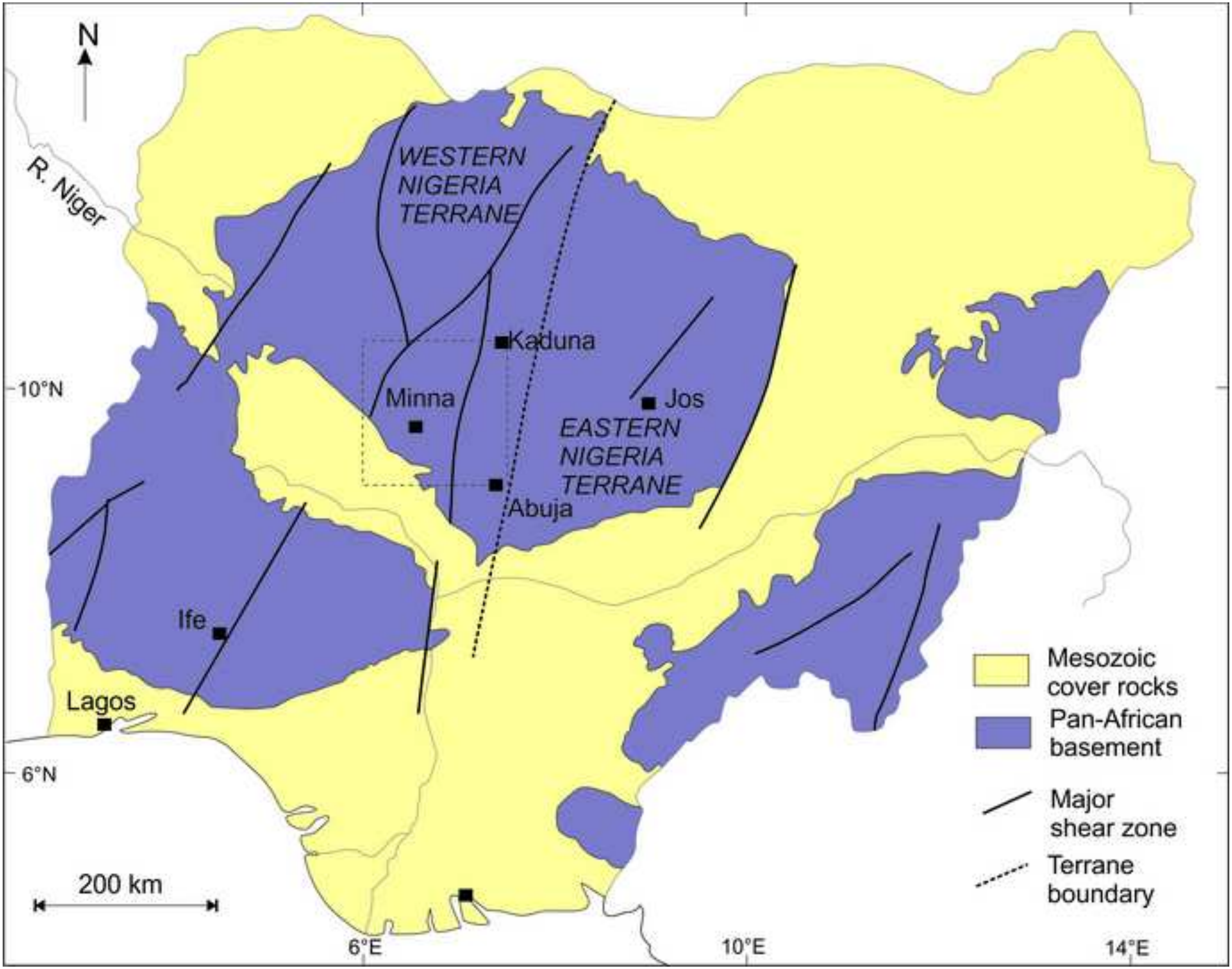

Figure 2
Click here to download high resolution image

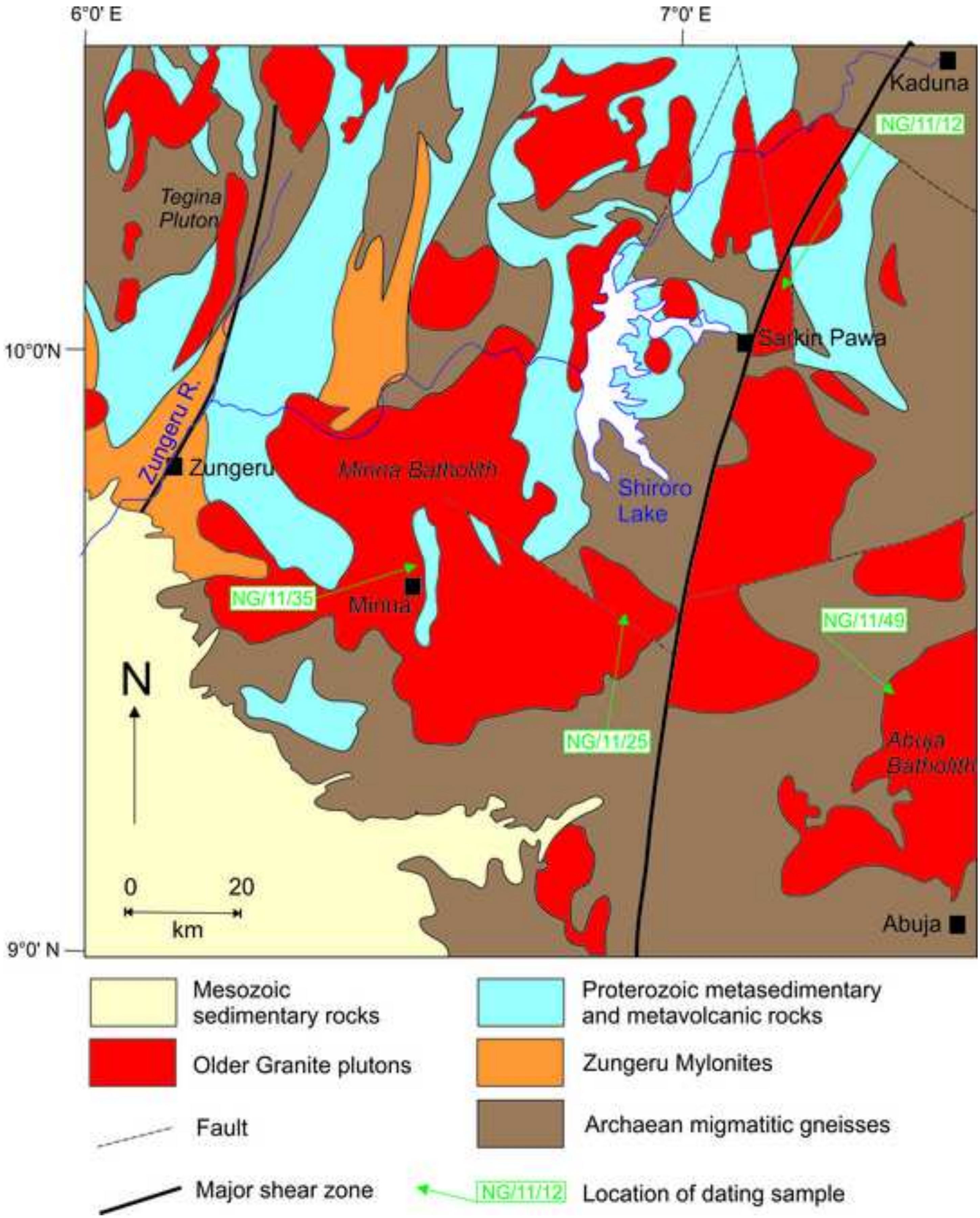

Figure 3
Click here to download high resolution image

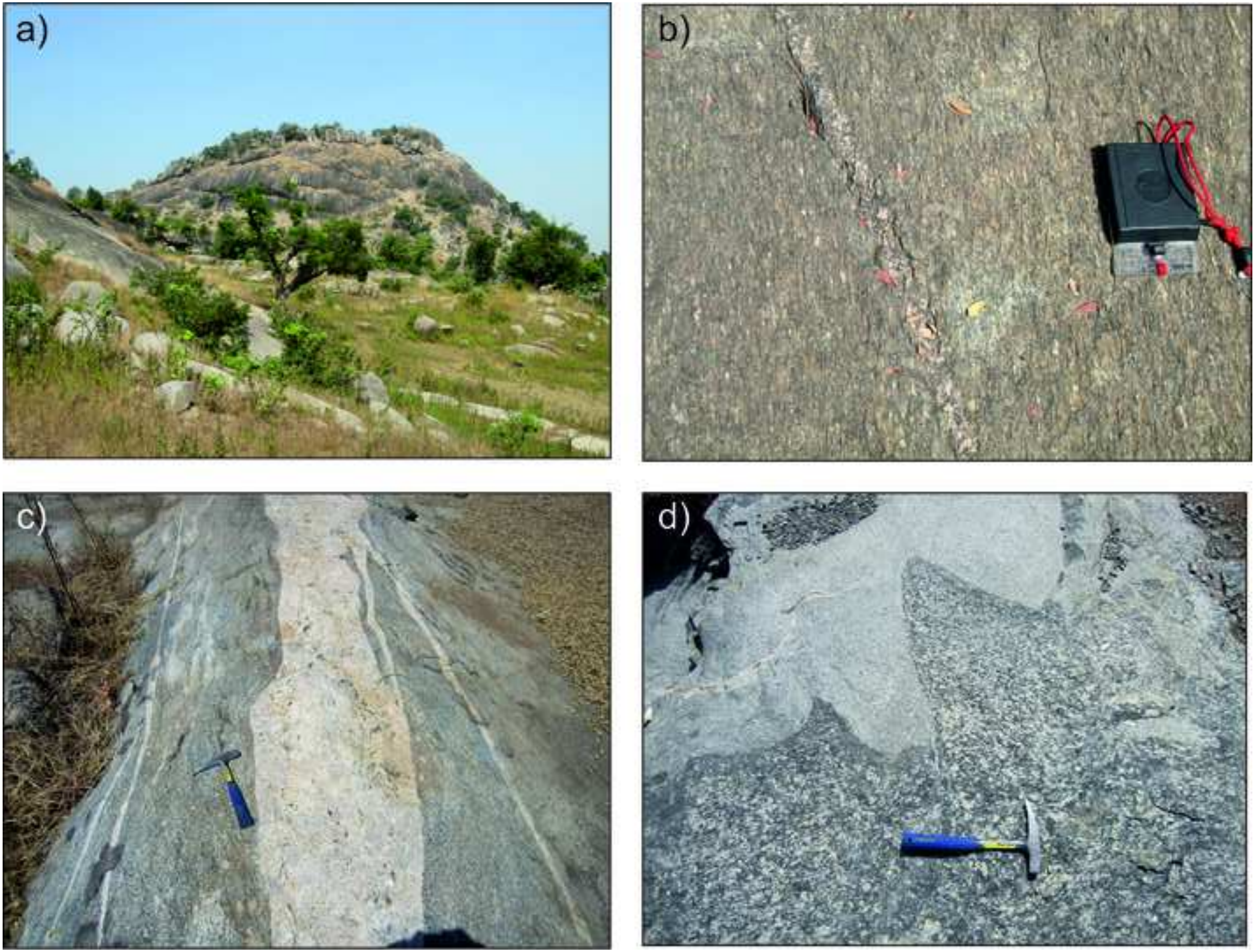

Figure 4

Click here to download high resolution image

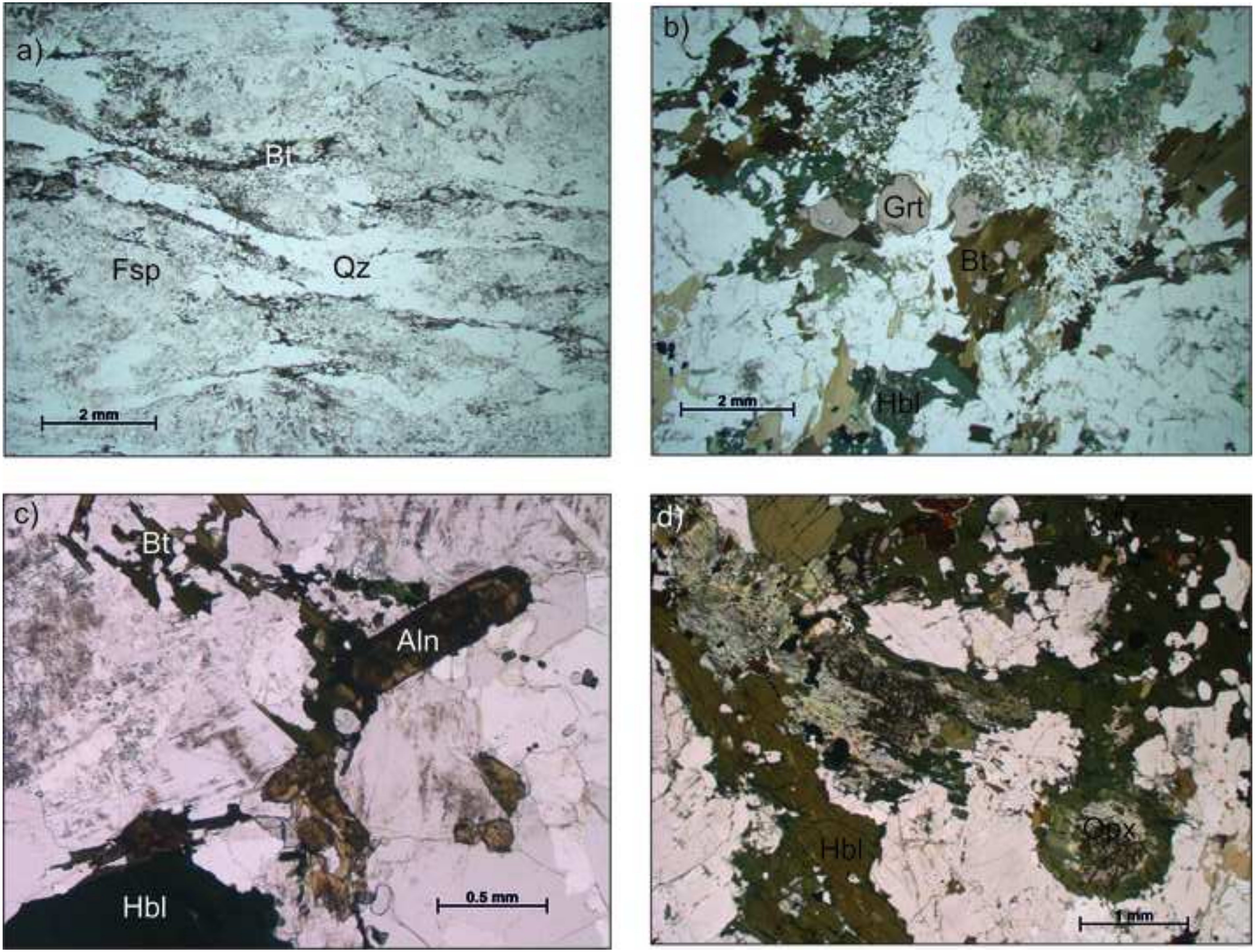

Figure 5
Click here to download high resolution image

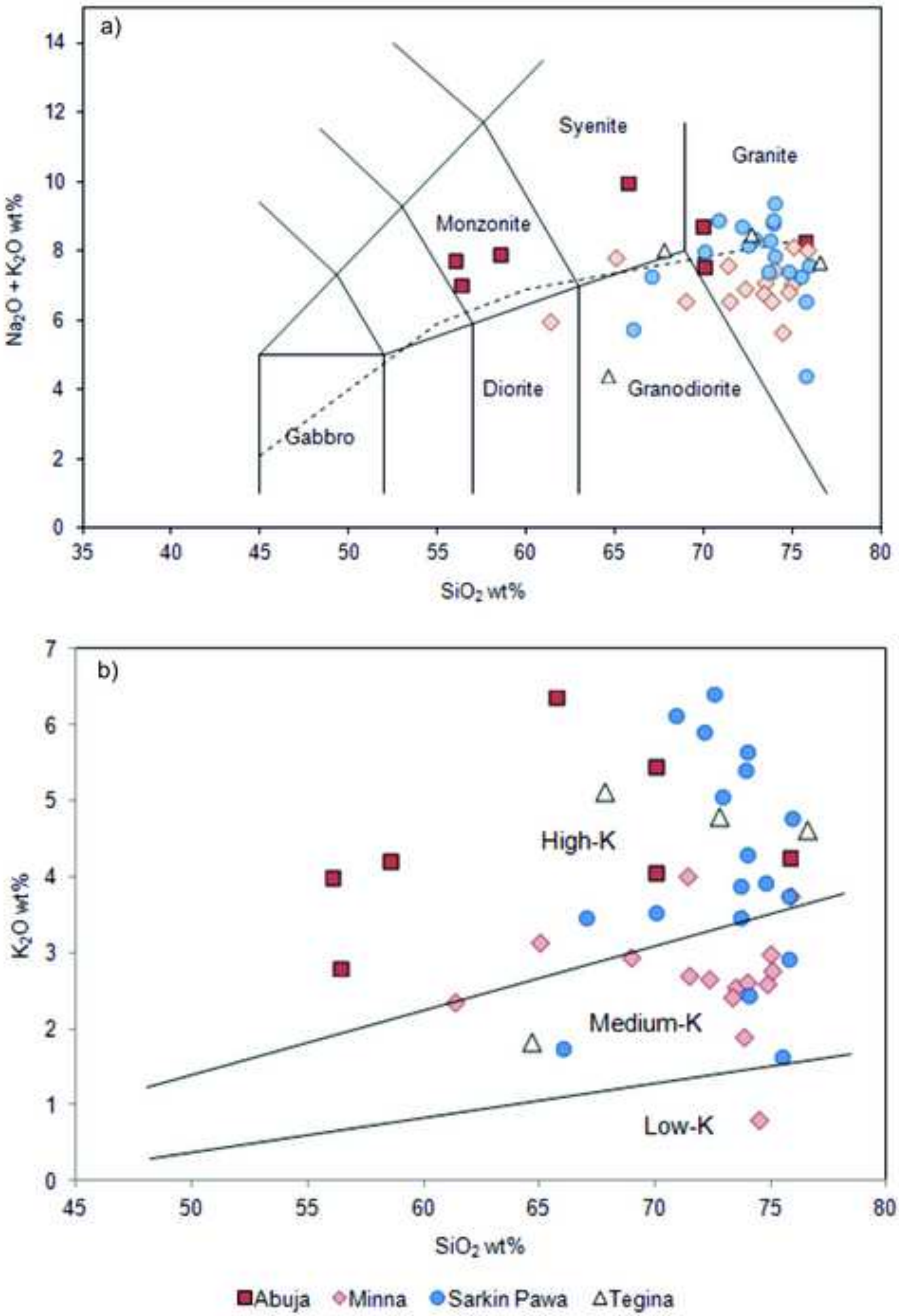

Figure 6
Click here to download high resolution image

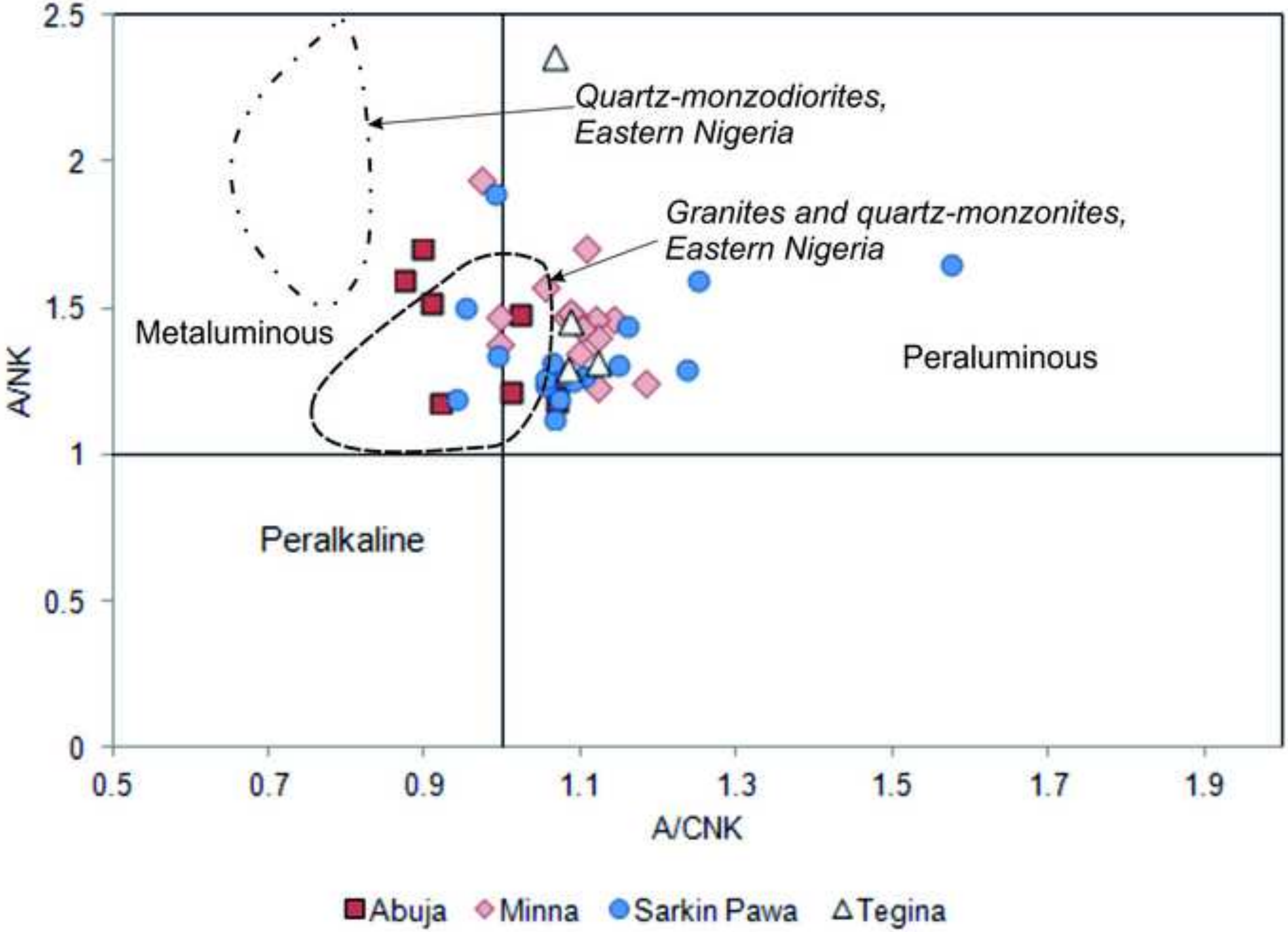

Figure 7
Click here to download high resolution image

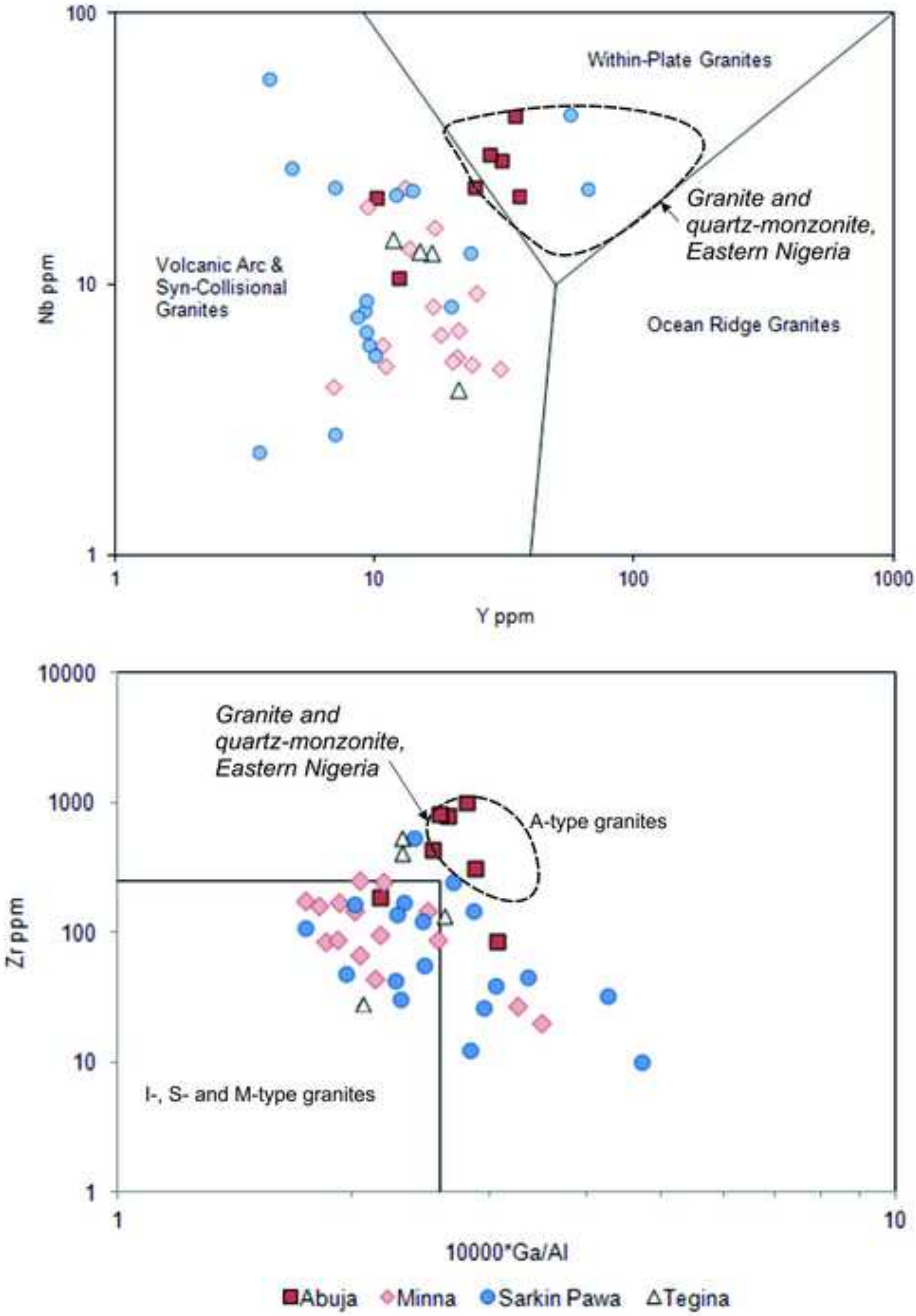

Figure 8
Click here to download high resolution image

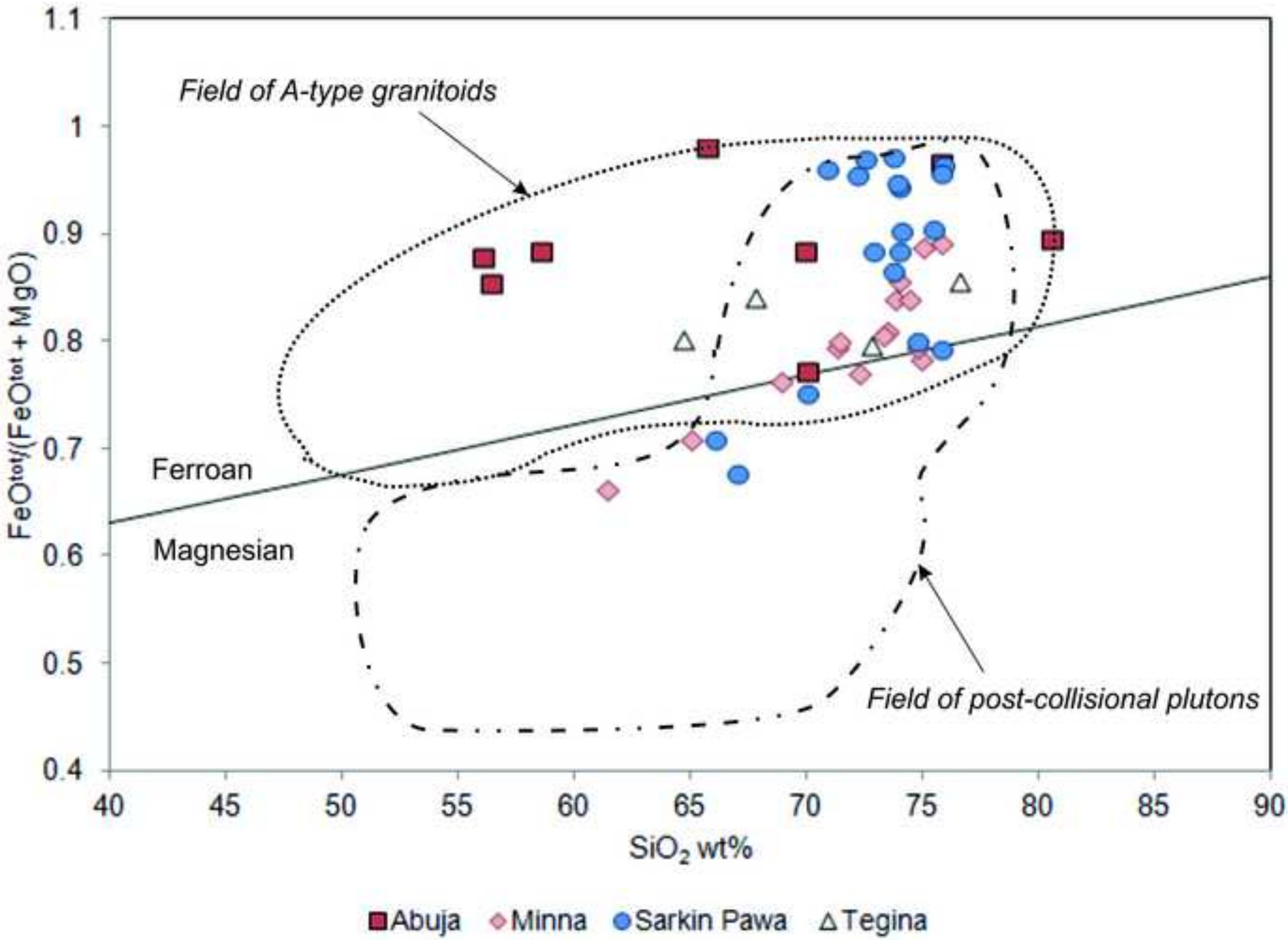

Figure 9
Click here to download high resolution image

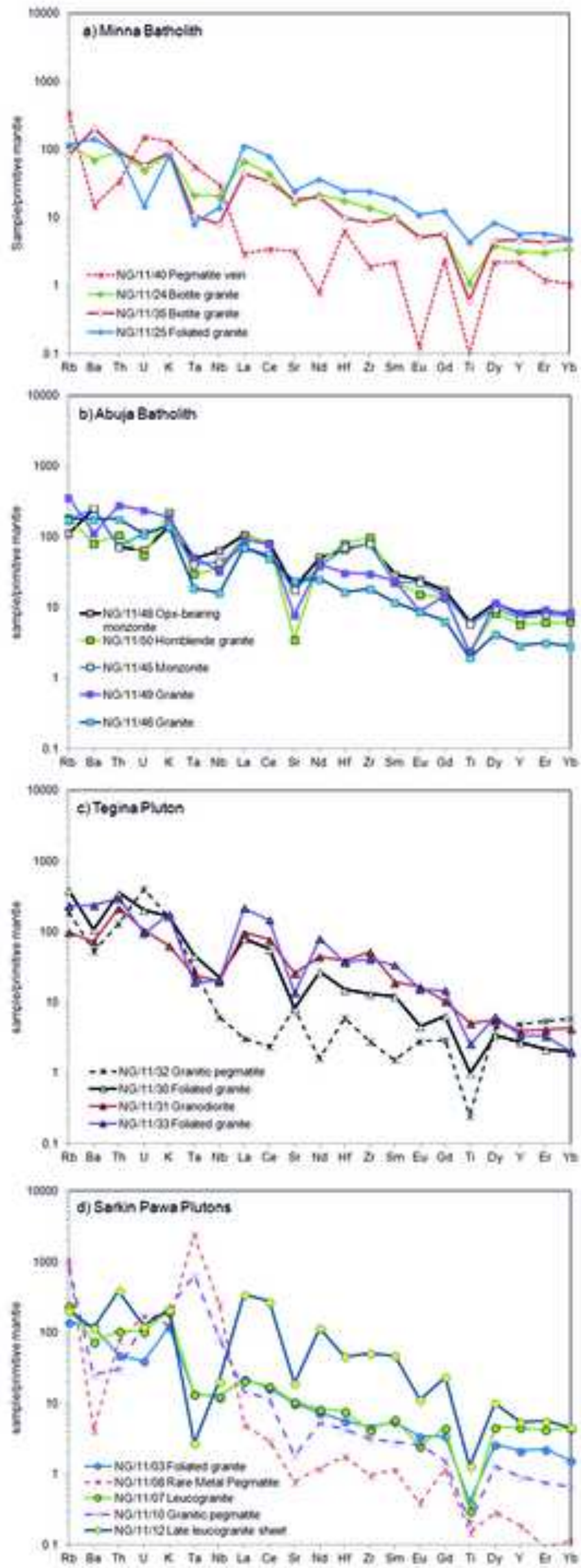

Figure 10
Click here to download high resolution image

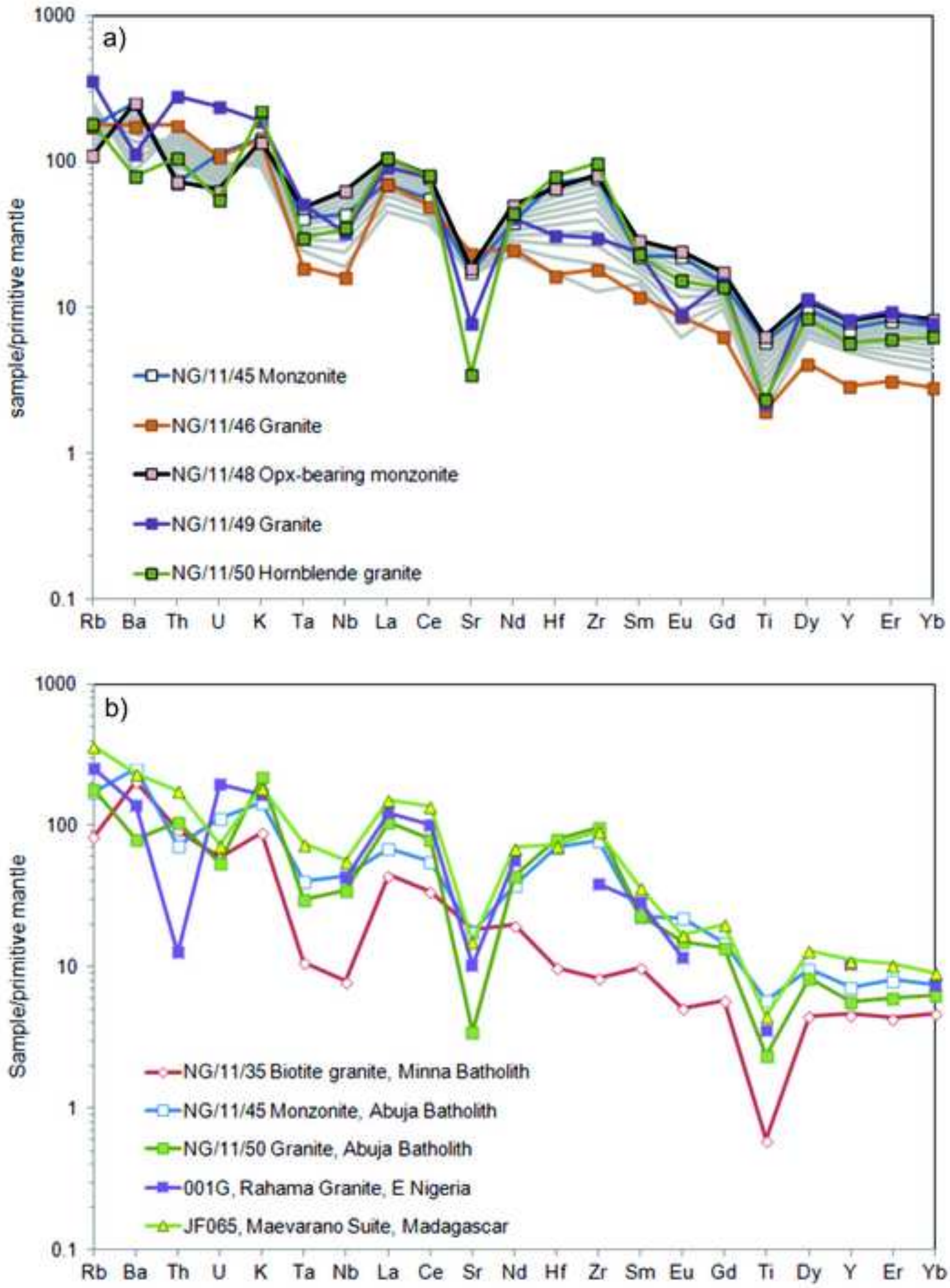

Figure 11
Click here to download high resolution image

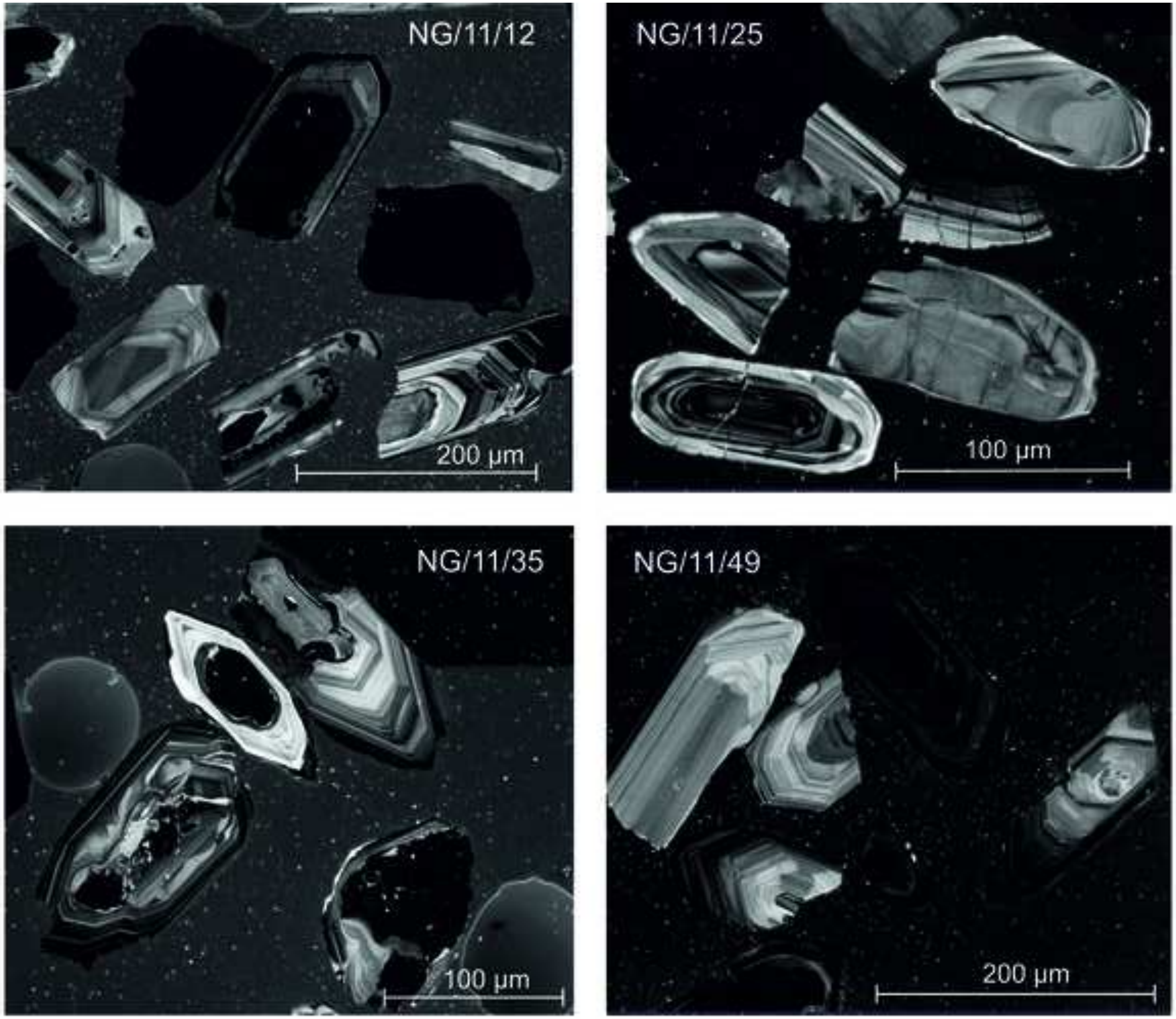

Figure 12

Click here to download high resolution image

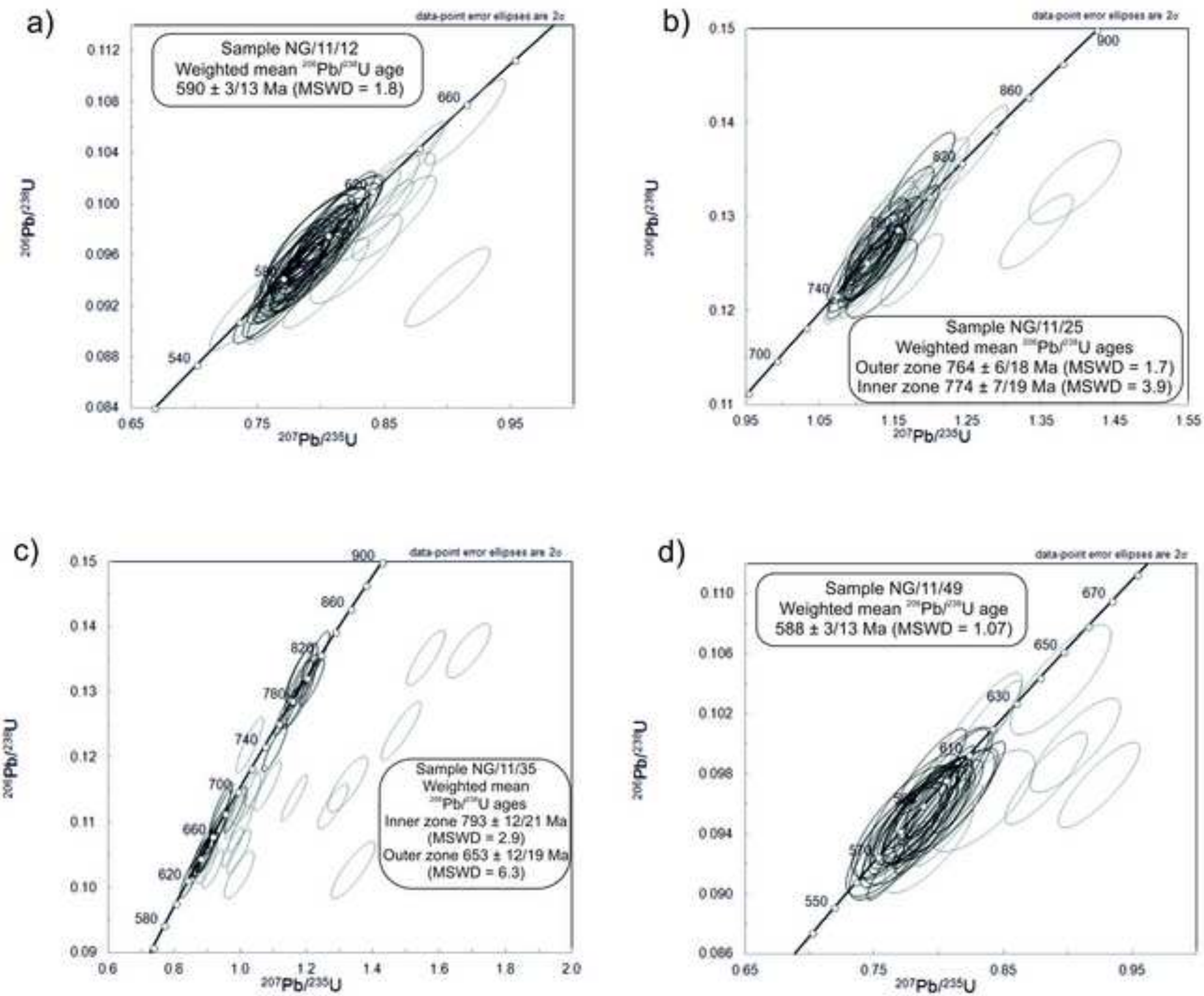

Table 1
Click here to download Table: Table1.xlsx

Sample	Rock type	Intrusion	SiO_2 %	Al_2O_3 %	Fe_2O_3 %	MgO %	CaO %
NG/11/1	Granite	Sarkin Pawa area	75.89	12.55	2.21	0.07	0.83
NG/11/2	Aplite	Sarkin Pawa area	73.68	15.01	1.15	0.03	0.34
NG/11/3	Granite	Sarkin Pawa area	73.65	14.81	1.44	0.2	1.38
NG/11/4	Diorite	Sarkin Pawa area	66.02	16.2	4.24	1.56	4.3
NG/11/5	Pegmatite	Sarkin Pawa area	75.44	14.56	0.97	0.09	0.9
NG/11/6	Pegmatite	Sarkin Pawa area	74	14.45	0.94	0.09	1.16
NG/11/7	Granite	Sarkin Pawa area	73.91	14.35	0.95	0.11	0.99
NG/11/8	Pegmatite	Sarkin Pawa area	75.73	16.08	1.25	0.05	0.01
NG/11/9	Granite	Sarkin Pawa area	72.87	14.02	2.22	0.26	1.15
NG/11/10	Pegmatite	Sarkin Pawa area	72.5	16.38	1.09	0.03	0.29
NG/11/11	Granite	Sarkin Pawa area	72.1	14.07	2.6	0.11	1.26
NG/11/12	Granite	Sarkin Pawa area	70.84	13.42	3.8	0.14	1.66
NG/11/13	Granite	Sarkin Pawa area	70.02	15.13	2.29	0.68	2.22
NG/11/14	Pegmatite	Sarkin Pawa area	73.94	14.74	0.76	0.04	0.44
NG/11/15	Granite	Sarkin Pawa area	66.99	15.12	3.86	1.65	3.21
NG/11/16	Gneiss	Country rock	71.12	14.47	3.09	0.82	2.01
NG/11/17	Granite	Sarkin Pawa area	73.87	13.94	1.82	0.09	0.74
NG/11/18	Granite	Sarkin Pawa area	74.74	13.28	1.47	0.33	1.35
NG/11/19	Granite	Sarkin Pawa area	75.74	14.69	0.73	0.17	1.42
NG/11/20	Gneiss	Country rock	53.92	19.23	7.02	3.04	4.95
NG/11/21	Granite	Minna Batholith	73.48	15.12	1.2	0.25	1.63
NG/11/22	Granodiorite	Minna Batholith	68.94	15.7	3.13	0.87	2.76
NG/11/23	Granite	Minna Batholith	71.36	15.2	1.82	0.42	2.09
NG/11/24	Granite	Minna Batholith	73.33	14.49	2.05	0.44	1.73
NG/11/25	Granodiorite	Minna Batholith	61.36	16.59	5.9	2.68	4.7
NG/11/26	Granite	Minna Batholith	74.93	14.09	1.01	0.25	1.41
NG/11/27	Granite	Minna Batholith	64.99	16.46	4.15	1.52	2.99
NG/11/28	Amphibolite	Country rock	48.4	17.76	8.37	6.06	10.71
NG/11/29	Mylonite	Country rock	72.39	14.26	2.89	0.58	2.51
NG/11/30	Granite	Tegina Granite	72.73	14.59	1.43	0.33	1.21
NG/11/31	Diorite	Tegina Granite	64.66	14.79	7.76	1.73	4.16
NG/11/32	Pegmatite	Tegina Granite	76.55	13.27	0.46	0.07	0.95
NG/11/33	Granodiorite	Tegina Granite	67.78	15.13	4.49	0.76	1.93
NG/11/34	Granite	Minna Batholith	73.83	14.48	1.65	0.28	1.92
NG/11/35	Granite	Minna Batholith	74.78	14.1	1.22	0.28	1.65
NG/11/36	Granite	Minna Batholith	74.44	13.24	2.98	0.51	1.83
NG/11/37	Amphibolite	Country rock	52.21	13.36	11.97	3.89	8.75
NG/11/38	Granite	Minna Batholith	73.95	14.69	1	0.15	1.38
NG/11/39	Aplite	Minna Batholith	75.04	14.61	0.54	0.06	0.66
NG/11/40	Pegmatite	Minna Batholith	75.84	13.96	0.65	0.07	0.36
NG/11/41	Granite	Minna Batholith	72.29	13.72	2.87	0.76	2.14
NG/11/42	Granite	Minna Batholith	71.41	14.79	2.57	0.57	2.58
NG/11/43	Leucogranite	Abuja batholith	75.76	13.34	0.98	0.03	0.67
NG/11/44	Pegmatite	Abuja batholith	80.49	10.06	0.96	0.1	0.94
NG/11/45	Diorite	Abuja batholith	58.51	16.18	9.78	1.13	3.95
NG/11/46	Granodiorite	Abuja batholith	70.01	15.05	2.73	0.72	2.53
NG/11/47	Diorite	Abuja batholith	56.34	17.05	10.14	1.53	4.97
NG/11/48	Diorite	Abuja batholith	56.03	16.72	10.42	1.28	4.76

Table 2

Click here to download Table: Table2.xlsx

Sample	Spot	comments	rejected?	^{204}Pb	^{206}Pb	^{207}Pb	^{208}Pb	^{232}Th	^{235}U	Th/U	Pbppm	Thppm
NG/11/12	5	bright osci outer		166	162989	9796	14209	301627	13206	0.28	41	112
NG/11/12	6	bright osci intermediate		-24	85065	5085	11173	227028	6799	0.41	22	85
NG/11/12	8	bright osci inner		165	200089	12295	38663	776381	17442	0.55	51	289
NG/11/12	9	bright osci inner		386	319230	19682	73800	1417362	26876	0.65	81	528
NG/11/12	10	bright osci outer		-20	111381	6741	11846	241742	9199	0.33	28	90
NG/11/12	14	bright osci outer		-2	128770	7952	17791	370356	10698	0.43	33	138
NG/11/12	15	bright osci intermediate		338	291642	18034	58509	1220460	26115	0.58	74	455
NG/11/12	16	bright osci inner		90	1006347	62136	128542	2796366	88112	0.39	255	1042
NG/11/12	17	bright osci outer		67	110691	6734	11970	258384	9641	0.33	28	96
NG/11/12	18	bright osci inner		37	178711	11040	35566	773294	15615	0.61	45	288
NG/11/12	19	bright osci outer		218	79649	4894	9498	212405	6915	0.38	20	79
NG/11/12	23	bright planar zoning inner		139	156886	9672	34178	794414	14209	0.69	40	296
NG/11/12	25	bright osci outer		278	122377	7483	18482	421820	11099	0.47	31	157
NG/11/12	27	bright osci outer		46	201146	12490	20141	482547	18877	0.32	51	180
NG/11/12	29	bright angular osci inner		406	97048	6007	7010	167188	8807	0.23	25	62
NG/11/12	30	bright osci intermediate		70	220584	13368	32847	812736	19915	0.50	56	303
NG/11/12	31	bright osci outer		182	132055	8150	13501	325795	12065	0.33	33	121
NG/11/12	32	bright altered zoning inner		-53	117954	7302	284	3599	10930	0.00	30	1
NG/11/12	34	bright osci outer		256	104008	6469	14407	383797	9908	0.48	26	143
NG/11/12	35	dark faint zoning		385	608530	37561	122705	3188862	58715	0.67	154	1189
NG/11/12	36	planar zoning inner		96	273323	17234	16695	380055	26310	0.18	69	142
NG/11/12	41	bright osci outer		257	78334	4815	11339	308608	7861	0.49	20	115
NG/11/12	43	bright osci inner		82	240236	14901	36581	925265	23959	0.48	61	345
NG/11/12	46	bright osci outer		47	84446	5281	10569	274508	8756	0.39	21	102
NG/11/12	47	bright osci intermediate		98	145033	8943	29344	819044	15004	0.68	37	305
NG/11/12	48	bright osci intermediate		239	115498	7108	25460	667685	11681	0.71	29	249
NG/11/12	49	bright osci inner		112	110140	6894	21561	595275	11239	0.66	28	222
NG/11/12	50	bright osci outer		280	106377	6787	12917	342315	11004	0.38	27	128
NG/11/12	51	bright osci intermediate		-29	212178	13264	31027	802188	21423	0.46	54	299
NG/11/12	52	bright osci inner		22	325221	19720	70709	1555266	26744	0.72	82	580
NG/11/12	53	bright osci outer		10	136826	8348	15504	346556	11379	0.38	35	129
NG/11/12	54	bright osci outer		85	211384	12976	37203	837781	17599	0.59	54	312
NG/11/12	55	bright osci inner		84	360931	21789	76981	1686699	29683	0.70	91	629
NG/11/12	56	bright osci outer		-51	145690	8901	14342	311247	12091	0.32	37	116
NG/11/12	57	bright osci intermediate		115	155024	9523	33710	739883	12828	0.71	39	276
NG/11/12	58	bright osci intermediate		-176	177951	10766	39905	900580	15120	0.74	45	336
NG/11/12	72	bright osci inner		56	245661	14495	49429	993577	19994	0.58	62	365
NG/11/12	74	dark osci inner		33	545624	33352	84395	1648605	43478	0.44	137	606
NG/11/12	76	dark osci inner		193	1064569	63846	172033	3203850	83450	0.45	267	1178
NG/11/12	78	bright osci outer		149	168583	10292	22921	423868	13572	0.36	42	156
NG/11/12	79	bright osci outer		-118	178138	10707	3223	58272	14936	0.05	45	21
NG/11/12	44	bright osci outer/ embayment	younger grain	172	97005	5953	1713	46561	10253	0.06	25	17
NG/11/12	1	bright osci outer	possible older inheritance	217	133961	8264	17786	345139	10557	0.40	34	129
NG/11/12	4	dark inner	possible older inheritance	258	2048359	127538	170718	3163079	148388	0.26	519	1179
NG/11/12	21	bright osci inner	possible older inheritance	77	144555	10809	44952	587601	7430	0.98	37	219
NG/11/12	22	dark osci outer	possible older inheritance	244	834532	52748	18693	393468	69269	0.07	211	147
NG/11/12	75	dark osci inner	possible older inheritance	277	653023	39652	46152	855818	51537	0.19	164	315
NG/11/12	80	bright osci outer	possible older inheritance	-72	167621	10508	10662	184021	13000	0.17	42	68
NG/11/12	2	dark inner	high discordance	134	3278566	205647	267773	5298838	272200	0.24	831	1975
NG/11/12	7	bright osci inner	high discordance	129	198757	13009	42099	783095	16502	0.59	50	292
NG/11/12	24	dark inner	high discordance	435	1582359	100797	180579	4031378	140630	0.35	401	1503
NG/11/12	33	bright osci intermediate	high discordance	348	172676	12434	40490	911183	16595	0.68	44	340
NG/11/12	42	dark osci inner	high discordance	231	3412982	214529	324764	8746103	351367	0.31	865	3260
NG/11/12	71	bright osci inner	high discordance	258	122257	7806	23980	430830	10038	0.50	31	158
NG/11/25	2	inner	included within inner zone age calc	-123	438305	29250	82831	1612383	26258	0.45	59	266
NG/11/25	5	inner	included within inner zone age calc	81	456884	30234	114312	1827496	30318	0.44	61	302
NG/11/25	6	inner	included within inner zone age calc	141	186406	12365	45229	738044	11868	0.43	25	122
NG/11/25	8	inner	included within inner zone age calc	-130	121889	7855	12535	191793	7597	0.18	16	32
NG/11/25	9	mixed	included within inner zone age calc	66	229468	14862	36049	534447	14433	0.27	31	88
NG/11/25	10	inner	included within inner zone age calc	20	185878	12010	36254	532509	11811	0.34	25	88
NG/11/25	12	inner	included within inner zone age calc	96	177187	11623	24180	354295	11188	0.23	24	59
NG/11/25	13	inner	included within inner zone age calc	22	209359	14067	36960	543712	13670	0.29	28	90
NG/11/25	15	inner	included within inner zone age calc	-4	314198	20919	63047	986459	19429	0.37	42	163
NG/11/25	16	inner	included within inner zone age calc	-18	256619	17144	39809	602898	16620	0.26	34	100
NG/11/25	17	inner	included within inner zone age calc	14	158591	10522	35802	525029	10030	0.38	21	87
NG/11/25	18	inner	included within inner zone age calc	94	257634	17035	48333	683556	15592	0.31	35	113
NG/11/25	19	inner	included within inner zone age calc	15	255168	16639	43601	603112	16263	0.26	34	100
NG/11/25	20	inner	included within inner zone age calc	115	363671	24168	93459	1335925	23498	0.42	49	221
NG/11/25	22	mixed	included within inner zone age calc	139	145168	9752	20920	318924	9508	0.24	20	53
NG/11/25	23	inner	included within inner zone age calc	-152	268977	17763	49008	748090	17871	0.30	36	124
NG/11/25	25	inner	included within inner zone age calc	198	429610	28928	105309	1657404	27028	0.43	58	274
NG/11/25	26	inner	included within inner zone age calc	70	231497	15409	57808	956993	15061	0.45	31	158
NG/11/25	27	inner	included within inner zone age calc	-132	286047	18798	57032	928721	18983	0.36	38	153
NG/11/25	28	mixed	included within inner zone age calc	54	85394	5639	12278	218023	5351	0.29	11	36